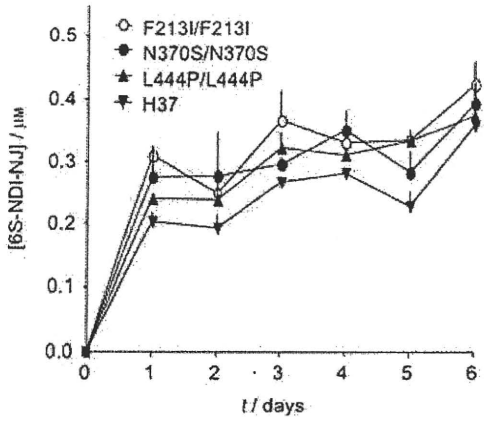

Figure 4. Expulsion of 6S-NDI-NJ from living fibroblasts. Living GD fibroblasts were incubated with 30 μM 6S-NDI-NJ for four days, then washout. The cells were further cultured for 1–6 d. The medium was aspirated for measurement of 6S-NDI-NJ concentration at indicated time. 6S-NDI-NJ medium was measured as described in experimental section.

and mature neurons respectively. We found that 6S-NDI-NJ can enter both immature and mature neurons after four days' incubation (Figure 6B). Additionally, 6S-NDI-NJ showed no toxicity on neuronal cells at a maximum concentration of 10 μM, whereas both intact and lysate assays showed that 6S-NDI-NJ enhanced β-Glu activities of neuronal cells, the maximum chaperone activity being reached at 1 μM concentration (Figure 6A). At higher concentrations the chaperone effect is counterbalance by the inhibitory effect, which becomes predominant at 10 μM.

High concentrations of glucose do not competitively inhibit cellular uptake of 6S-NDI-NJ

At present, there is no information about the cellular uptake pathways of chemical chaperones. Considering the structural similarity of the polyhydroxylated cyclic nojirimycin framework and D-glucose, it seemed reasonable that this family of compounds might share the cell-uptake mechanisms through glucose-specific transporters. Notwithstanding, we found that the presence of D-glucose at 25, 50, and 100 mM in the incubation medium had no influence on the intracellular fluorescent intensities of 6S-NDI-NJ in the human normal fibroblasts (data not shown). The absence of competitive inhibition by D-glucose in the internalization of 6S-NDI-NJ suggests that the chemical chaperone enters the cells through glucose-transporter-independent mechanisms.

Discussion

To circumvent the limitations of ERT and SRT to neurological manifestations, new therapeutic avenues for GD have been explored in recent years.[5,6] Chemical chaperone therapy is a promising approach because of its potential for simple oral administration, penetration of the blood–brain barrier, and low cost. Chaperones are small molecules that can specifically bind to a misfolded protein and help it fold into the correct three-dimensional shape. This allows the protein to be properly trafficked from the ER and distributed to the lysosome in the cell, thereby increasing enzyme activity and cellular function and reducing substrate and stress on cells.[47,48] Up to now, a broad battery of chemical chaperones has been developed for GD, including both sugar-like and non-sugar-related molecules. Recently, we found that bicyclic derivatives featuring a 2-iminooxazolidine, -thiazolidine, or imidazolidine five-membered ring fused to a polyhydroxylated pyperidine cycle, termed sp^2-iminosugars, behaved as selective competitive inhibitors of the lysosomal β-Glu and exhibited significant chaperone activity for several neuronopathic GD mutations.[30]

Although the concentration of mutant GD proteins in the lysosome has been shown to be enhanced by the presence of chemical chaperones, thereby supporting the proposed rescuing mechanism, to the best of our knowledge there is no direct information available about the intracellular distribution and cellular uptake pathways of such compounds. To clarify these questions, we have synthesized a fluorescently tagged version of the previously reported bicyclic nojirimycin sp^2-iminosugars NOI-NJ, 6S-NOI-NJ, and 6N-NOI-NJ, namely 6-thio-(5*N*,6*S*)-[4-(*N*'-dansylamino)butyliminomethylidene]nojirimycin (6S-NDI-NJ). Actually, the general approach previously developed for the synthesis of bicyclic nojirimycin derivatives of the sp^2-iminosugar type was purposely conceived to allow introduction of molecular diversity in the structure at a relatively low synthetic cost.

In the molecular design of 6S-NDI-NJ, we took advantage of the information previously obtained from X-ray crystallography and thermodynamic studies on bicylic sp^2-iminosugars in complex with recombinant human β-glucocerebrosidase[29] or with the β-glucosidase from the extremophile microorganism *Thermotoga maritima*,[28] an enzyme that belongs to the same clan GHA as β-Glu in the CaZy classification.[48] The octyl chain at the exocyclic nitrogen of NOI-NJ, 6S-NOI-NJ, or 6N-NOI-NJ (Scheme 1) in the enzyme–inhibitor complexes was found to occupy a hydrophobic pocket at the entrance of the active site in all cases, while maintaining substantial flexibility. It was then inferred that structural modifications at this portion of the molecule would not affect the extensive hydrogen-bond network involving the hydroxyl groups and would be well tolerated as far as its hydrophobic nature is preserved. The 6-thio-5*N*,6*S*-(alkyliminomethylidene)nojirimycin bicyclic core was chosen in view of the good chaperone activities previously obtained with 6S-NOI-NJ for several mutant β-Glu. Moreover, the isothiourea segment can be generated with high efficiency from a *vic*-hydroxythiourea intermediate **2**, which is readily accessible from the known 5-amino-5-deoxy-D-glucofuranose derivative **1** by activation of the OH function as a sulfonate ester followed by nucleophilic displacement by the thiocarbonyl sulfur atom (→**3**). The subsequent furanose→pyranose rearrangement is a very efficient process that affords the desired bicyclic sp^2-iminosugar core **4**. The terminal amino group in the N-alkyl substituent in **4** was then exploited for the incorporation of the fluorescent probe in the structure by coupling reaction with dansyl chloride (Scheme 2).

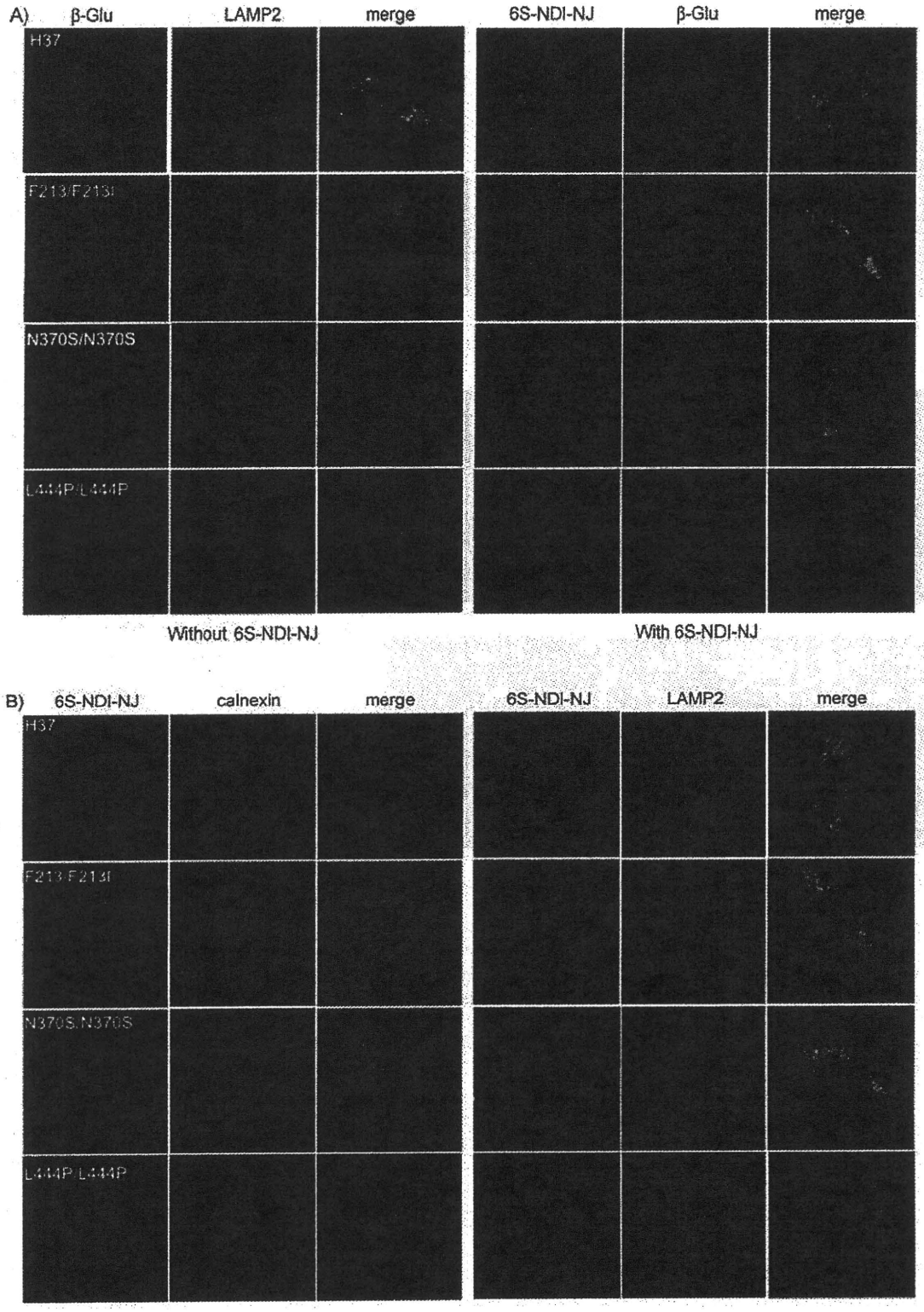

Figure 5. Intracellular distribution of 6S-NDI-NJ in GD fibroblasts. A) Cells in the absence or the presence of 6S-NDI-NJ (30 μM) were double stained with anti β-Glu and LAMP2 antibody or anti β-Glu antibody. B) The cells were cultured for 4 d in the presence of 6S-NDI-NJ (30 μM) and stained with anti-calnexin antibody or anti-LAMP2 antibody. Bound antibodies were visualized with different secondary antibody. The images obtained with a confocal microscope are shown.

First, we confirmed that the insertion of the dansyl group was not detrimental for the biological activity. According to the collected data, 6S-NDI-NJ is a specific inhibitor of β-Glu (Figure 1), exhibits no cytotoxicity at the maximum assayed concentration of 30 μM in human fibroblasts, and can enhance β-Glu activities in human F213I/F213I and N370S/N370S GD fibroblasts (Figure 2). All these characteristics are similar to those previously reported for 6S-NOI-NJ.[30] Moreover, fluores-

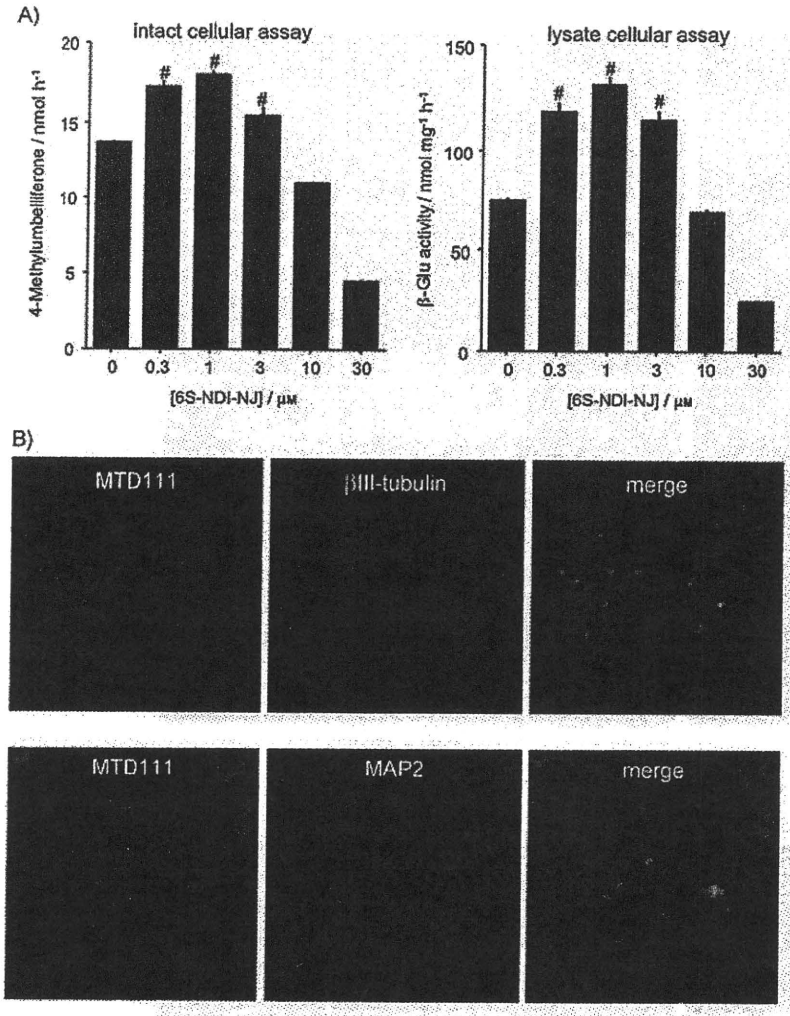

Figure 6. The effect of 6S-NDI-NJ on neuronal cells differentiated from P19 EC cells. A) Enzyme assay. Neuronal cells were cultured for 4 d in the absence or presence of increasing concentrations of 6S-NDI-NJ. β-Glu activity was estimated in intact cells and lysate as described in the Experimental Section. $^{\#}p < 0.01$ highly significant, statistically different from the values in the absence of the compound (t-test). B) The immature and mature neuronal cells were cultured for 4 d in the presence of 6S-NDI-NJ (30 μM) and stained with anti-βIII-tubulin antibody and anti-MAP2 antibody. Bound antibodies were visualized with a different secondary antibody. Shown are the images obtained with a confocal microscope.

cence spectroscopy measurements showed that the spectral properties of 6S-NDI-NJ in aqueous and organic media were well suited for studies of the interactions of this molecule with cultured cells.

Prior to examining the ability of 6S-NDI-NJ to increase the concentration of mutant β-Glu in the lysosome, we examined its capacity to attenuate time-dependent loss of mutant β-Glu activity in vitro at pH 7 at 37 and 48 °C. This protecting effect has been shown to be an indication of good chaperone capabilities, and was ascribed to its efficiency in forcing a correct folding.[46,49] The GD mutants F213I/F213I and N370S/N370S are not stable in the neutral pH environment of the ER and undergo endoplasmic-reticulum-associated degradation (ERAD) to a great extent. In vitro experiments showed that the degradation rate at pH 7.0 at either 37 °C or 48 °C in vitro dramatically decreased in the presence of the dansyl derivative 6S-NDI-NJ. On the contrary, the L444P/L444P mutant protein was found to be as stable as the wild-type (WT) β-Glu at pH 7.0 at 37 °C and also showed similar activity, in agreement with previous results by Sawkar et al.[46] Heat denaturation at 48 °C was also efficiently attenuated by 6S-NDI-NJ in the WT and the L444P/L444P mutant. Nevertheless, the Ig-like domain in which the L444P mutation is located is not tolerated, and, although it does not cause instability associated with the neutral pH, the mutant β-Glu is still subjected to ERAD leading to degradation of the entire enzyme. Actually, the results in Figure 2 further supports that location of the mutation responsible for GD in the catalytic domain of β-Glu (domain III), which is the case of the F213I/F213I and N370S/N370S but not of the L444P/L444P mutant, is a prerequisite for the pharmacological rescue of the protein by an active-site-directed chemical chaperone.

Fluorescence microscopy evidenced that the dansyl-tagged chaperone 6S-NDI-NJ enters the cells upon incubation. Conversely, washout of the culture medium resulted in a gradual decrease of fluorescence intensity in the living cells (data not shown) and a concomitant increase in the concentration of 6S-NDI-NJ in the fresh culture medium (Figure 4). The sp^2-iminosugar can therefore be internalized and further released from fibroblasts into the surrounding medium.

Intracellular distribution studies of 6S-NDI-NJ showed that in GD and normal fibroblasts the chaperone co-localized with β-Glu and was mainly distributed in lysosome-associated organelles, the dansyl-associated fluorescent intensity correlating with the β-Glu protein level. These data are in agreement with the observed binding selectivity of 6S-NDI-NJ towards β-Glu. It should be noted that once in the lysosome the chaperone might attenuate β-Glu activity by their enzyme-inhibitory activity. Although iminosugar and sp^2-iminosugar-type chemical chaperones both exhibit generally higher affinities for WT and mutant β-Glu at neutral than at acidic pH, this feature has previously been found to be significantly more pronounced in the case of the sp^2-iminosugars.[30,50] This probably results in comparatively stronger binding to the mutant enzymes at the ER, where the chaperone activity must operate for rescuing the enzyme from ERAD, than in the lysosome. Because they act as competitive inhibitors, once in the lysosome the high concentrations of substrate accumulated in GD cells will compete with the inhibitor in binding to the enzyme.[45]

Given that chemical chaperone therapy by using sp^2-iminosugar glycomimetics was proposed mainly for neuronopathic GD, it was of interest to investigate the effect of 6S-NDI-NJ in neurons. For this purpose, we have used cultured normal neuronal cells, which were differentiated from P19 embryonal carcinoma cells. We found that 6S-NDI-NJ could enter immature and mature neurons after four-days incubation and enhanced β-Glu activities, with a maximum chaperone effect at 1 μM

concentration, compared to 30 μM in fibroblasts. It seems that neuronal cells are much more sensitive to chaperone therapy. Because a much lower concentration of chaperone in the CNS than in peripheral tissues is expected upon oral administration,[17] the possibility to use relatively high doses of sp²-iminosugars might result in optimal chaperone activity simultaneously in both types of tissues, making them potentially more practical for the treatment of neuronopathic GD.

In addition to intracellular localization studies, the fluorescently labeled chemical chaperone 6S-NDI-NJ provides an excellent opportunity to explore the preferred cellular uptake pathways of sp²-iminosugars. Considering that the piperidine ring in 6S-NDI-NJ has a hydroxylation profile of stereochemical complementarity with that of D-glucose, it seemed reasonable to consider that it might share identical internalization mechanisms. Because D-glucose is a polar molecule that requires transport proteins to cross biological membranes, this would imply that the chaperone and the monosaccharide compete for the same transporters. Notwithstanding, we found that high concentrations of D-glucose did not result in competitive inhibition of 6S-NDI-NJ uptake, suggesting instead that the sp²-iminosugar enters the cells through glucose-transporter-independent pathways. The amphiphilic character of 6S-NDI-NJ and the previously studied sp²-iminosugar chemical chaperones, with a hydrophilic polyhydroxylated moiety and a hydrophobic substituent in the lateral chain, might facilitate passive diffusion across the cell membrane. Concentration gradient and β-Glu binding affinity would then trigger uptake and release of 6S-NDI-NJ. The fact that the chaperone co-localizes with acid β-Glu in lysosome-related organelles and that its concentration in the cell is closely related to the concentration of the enzyme is consistent with this mechanism. Alternative endocytic routes would be expected to lead primarily to localization of the internalized fluorescent chaperone in endosomes, independently of the β-Glu concentration. Further research using specific endocytosis inhibitors is currently underway to fully ascertain this aspect.

In summary, the present body of work provides evidence for the rescuing of GD β-Glu with mutations at the catalytic domain by sp²-iminosugars, facilitating trafficking from the ER to the lysosome. The concentration of the mutant enzyme in the lysosome correlated with the intracellular concentration of 6S-NDI-NJ both in fibroblasts and in neuronal cells, which underlines the importance of the internalization process in the efficiency of a chemical chaperone. Actually, when screening chemical chaperones we often found that some candidates with very low IC_{50} values against the target enzyme exhibited disappointingly low chaperone activity when using intact cells. Their inability to cross the cell membrane attenuates their chaperone activity. The amphiphilic character of the sp²-iminosugar chemical chaperones seems to favor a passive diffusion pathway that facilitates cell internalization. Structural modifications aimed at optimizing the hydrophilic/hydrophobic balance might further increase their ability to cross the cell membrane and improve their chaperone activity. Although further work is needed to fully unravel the relationships between molecular structure, cellular uptake pathways, and chaperone activity, these results should help to improve the present strategies for the development of efficient chemical chaperones.

Experimental Section

Materials: Dulbecco's modified Eagle's medium (DMEM) and fetal bovine serum (FBS) were obtained from Life Technologies Inc (Gibco BRL, MD, USA). Reagents and solvents were purchased from commercial sources and used without further purification. 6S-NDI-NJ was synthesized in our laboratories by following the reaction sequence described hereinafter. A stock solution of the compound was prepared in DMSO at 30 mM and stored at −30 °C.

Spectroscopic and chromatographic techniques: Optical rotations were measured with a JASCO P-2000 polarimeter, by using a sodium lamp ($\lambda = 589$ nm) at 22 °C in 1 cm or 1 dm tubes. NMR spectroscopy experiments were performed at 300 (75.5) and 500 (125.7) MHz by using Bruker DMX300 and DRX500 spectrometers. 1D TOCSY as well as 2D COSY and HMQC spectroscopy experiments were carried out to assist in signal assignment. In the FABMS spectra, the primary beam consisted of Xe atoms with a maximum energy of 8 keV. The samples were dissolved in *m*-nitrobenzyl alcohol or thioglycerol as the matrices, and the positive ions were separated and accelerated over a potential of 7 keV. NaI was added as cationizing agent. Thin-layer chromatography was performed on E. Merck precoated TLC plates, silica gel 30F-245, with visualization by UV light and by charring with 10% H_2SO_4 or 0.2% (*w/v*) cerium(IV) sulfate-5% ammonium molybdate in 2 M H_2SO_4 or 0.1% ninhydrin in EtOH. Column chromatography was performed on Chromagel (SdS silica 60 AC.C 70–200 μm). Elemental analyses were performed at the Servicio de Microanálisis del Instituto de Investigaciones Químicas de Sevilla.

Synthesis: The dansyl-tagged sp²-iminosugar 6S-NDI-NJ was synthesized from 5-amino-5-deoxy-1,2-di-*O*-isopropylydene-6-*O*-tetrahydropyranyl-α-D-glucofuranose (**1**) as indicated in Scheme 2. Compound **1** was generated from the corresponding 5-azido derivative[36] (700 mg, 2.13 mmol) by dissolution in MeOH (12 mL) and hydrogenation at atmospheric pressure for 1 h by using 10% Pd/C (234 mg) as a catalyst, and was used without further purification.[28]

5-[*N'*-(4-*tert*-Butoxycarbonylaminobutyl)thioureido]-5-deoxy-1,2-*O*-isopropylidene-α-D-glucofuranose (2): Et_3N (1.6 mL, 11.7 mmol) and 4-(*tert*-butoxycarbonylamino)butyl isothiocyanate (433 mg, 2 mmol) were added to a solution of **1** (2.13 mmol) in pyridine, (12 mL), and the mixture was stirred at RT for 18 h. The solvent was removed under reduced pressure, and the residue was co-evaporated several times with toluene. The resulting syrup was dissolved in CH_2Cl_2/MeOH (1:1, 42 mL) and *p*-toluenesulfonic acid (69 mg, 0.16 mmol) was added. The mixture was stirred for 2 h at RT, then diluted with CH_2Cl_2 (15 mL), washed with sat. aq $NaHCO_3$ (2×15 mL), dried ($MgSO_4$), filtered, and concentrated. The resulting residue was purified by column chromatography using 30:1→15:1 CH_2Cl_2/MeOH as eluent to give **2** (629 mg, 70%). $R_f = 0.33$ (15:1, CH_2Cl_2/MeOH); $[\alpha]_D = +45.5$ ($c = 1.0$ in CH_2Cl_2); ^{1}H NMR (300 MHz, $CDCl_3$, 313 K): $\delta = 6.96$ (brs, 1H; N'H), 6.72 (brd, $J_{NH,5} = 7.8$ Hz, 1H; NH), 5.92 (d, $J_{1,2} = 3.6$ Hz, 1H; H-1), 5.07 (brs, 1H; OH), 4.82 (brs, 1H; NH), 4.58 (d, 1H; H-2), 4.54 (m, 1H; H-5), 4.19 (d, $J_{3,4} = 1.9$ Hz, 1H; H-3), 4.09 (dd, $J_{4,5} = 9.8$ Hz, 1H; H-4), 4.03 (dd, $J_{6a,6b} = 11.3$ Hz, $J_{5,6a} = 3.1$ Hz, 1H; H-6a), 3.80 (dd, $J_{5,6b} = 3.0$ Hz, 1H; H-6b), 3.47 (m, 2H; CH_2NHCS), 3.11 (m, 2H; CH_2NHCO), 1.60 (m, 4H; CH_2), 1.49 (s, 3H; CMe_2), 1.31 (s, 3H; CMe_2), 1.49 ppm (s, 9H; CMe_3); ^{13}C NMR (75.5 MHz, $CDCl_3$, 313 K): $\delta = 181.8$ (CS), 156.7 (CO), 111.6 (CMe_2), 104.9 (C-1), 84.7 (C-2), 79.8 (CMe_3), 79.7 (C-4), 73.8 (C-3), 62.4 (C-6),

53.7 (C-5), 44.1 (CH_2NHCS), 40.2 (CH_2NHCO), 28.4 (CMe_3), 27.4 (CH_2), 26.7, 26.0 (CMe_2), 25.7 (CH_2); MS (FAB): *m/z* (%): 472 (100) $[M+Na]^+$, 450 (15) $[M+H]^+$; IR: $\tilde{\nu}_{max}$ = 3342, 2933, 1682, 1549, 1367, 1254, 1165, 1075 cm^{-1}; UV: $\lambda_{max}(CH_2Cl_2)$ = 247 nm (ε_{mM} = 12.3); elemental analysis calcd (%) for $C_{19}H_{35}N_3O_7S$: C 50.76, H 7.85, N 9.35, S 7.13; found: C 50.78, H 7.93, N 9.28, S 6.96.

(4*R*)-2-(4-*tert*-Butoxycarbonylamino)butylamino-4-[(4′*R*)-1′,2′-*O*-isopropylidene-β-L-threofuranos-4′-yl]-2-thiazoline (3): Methanesulfonic chloride (110 μL, 1.42 mmol, 1.2 eq) was added to a solution of the corresponding thioureido derivative **2** (514 mg, 1.14 mmol) in anhyd pyridine (17 mL) at −20 °C under argon. The mixture was stirred for 7 h and allowed to warm to RT. Then, ice-water (30 mL) was added, and the solution was extracted with CH_2Cl_2 (3×20 mL). The combined extracts were washed with iced sat. aq $NaHCO_3$ (25 mL), dried ($MgSO_4$), filtered, and concentrated. The resulting residue was purified by column chromatography by using 20:1→10:1 CH_2Cl_2/MeOH as eluent to give **3** (384 mg, 78%). $[\alpha]_D$ = −7.3 (*c* = 1.0 in CH_2Cl_2); R_f 0.46 (CH_2Cl_2/MeOH 7:1); ^{1}H NMR (300 MHz, $CDCl_3$): δ = 5.93 (d, $J_{1,2}$ = 3.6 Hz, 1H; H-1), 4.79 (brs, 1H; NH), 4.54 (d, 1H; H-2), 4.42 (m, 1H; H-5), 4.25 (brs, 2H; OH, NH), 4.23 (d, $J_{3,4}$ = 2.5 Hz, 1H; H-3), 4.03 (dd, $J_{4,5}$ = 8.4 Hz, 1H; H-4), 3.51 (dd, $J_{6a,6b}$ = 10.9 Hz, $J_{5,6a}$ = 7.4 Hz, 1H; H-6a), 3.39 (dd, $J_{5,6b}$ = 4.9 Hz, 1H; H-6b), 3.24 (m, 2H; CH_2N), 3.11 (m, 2H; CH_2NHCO), 1.53 (m, 4H; CH_2), 1.48 (s, 3H; CMe_2), 1.30 (s, 3H; CMe_2), 1.33 ppm (s, 9H; CMe_3); ^{13}C NMR(75.5 MHz, $CDCl_3$): δ = 164.6 (CN), 156.1 (CO), 111.5 (CMe_2), 105.1 (C-1), 85.2 (C-2), 81.6 (C-4), 79.3 (CMe_3), 74.9 (C-3), 69.8 (C-5), 44.9 (CH_2N), 40.0 (CH_2NHCO), 37.4 (C-6), 28.4 (CMe_3), 27.3, 26.8 (CH_2), 26.8, 26.1 ppm (CMe_2); IR: $\tilde{\nu}_{max}$ = 3372, 2934, 1696, 1521, 1367, 1251, 1166, 1075 cm^{-1}; MS (FAB): *m/z* (%): 454 (50) $[M+Na]^+$, 432 (100); elemental analysis calcd (%) for $C_{19}H_{33}N_3O_6S$: C 52.88, H 7.71, N 9.74, S 7.43; found: C 52.66, H 7.65, N 9.48, S 7.19.

5-*N*,6-*S*-[*N*′-(4-Amino)butyliminomethylidene]-6-thionojirimycin hydrochloride (4): The 2-amino-2-thiazoline precursor **3** (340 mg, 0.79 mmol) was treated with TFA/H_2O (9:1, 3.5 mL) for 30 min, concentrated under reduced pressure, coevaporated several times with H_2O, neutralized with Amberlite IRA-68 (OH^-) ion-exchange resin, and subjected to column chromatography by using 10:1:1 → 6:3:1 $CH_3CN/H_2O/NH_4OH$ as eluent. The residue was dissolved in dil HCl and freeze-dried to obtain compound **4** as the corresponding hydrochloride (258 mg, 82%). α/β = 1:0.1 (H-1 integration); R_f = 0.22 (6:3:1 $CH_3CN/H_2O/NH_4OH$) $[\alpha]_D$ = −11.3 (*c* = 1.0 in H_2O); α anomer: ^{1}H NMR (500 MHz, D_2O): δ = 5.61 (d, $J_{1,2}$ = 3.7 Hz, 1H; H-1), 4.32 (m, 1H; H-5), 3.76 (m, 2H; H-3, H-6a), 3.62 (dd, $J_{2,3}$ = 9.5 Hz, 1H; H-2), 3.56 (t, $J_{3,4}$ = $J_{4,5}$ = 9.6 Hz, 1H; H-4), 3.46 (m, 3H; H-6b, CH_2N), 3.00 (t, $^3J_{H,H}$ = 7.1 Hz, 2H; CH_2NH_2), 1.73 ppm (m, 4H; CH_2); ^{13}C NMR (125.7 MHz, D_2O): δ = 175.7 (CN), 79.0 (C-1), 75.7 (C-4), 74.2 (C-3), 73.1 (C-2), 66.0 (C-5), 50.6 (CH_2N), 41.5 (CH_2NH_2), 33.9 (C-6), 27.7, 26.5 ppm (CH_2); β anomer: ^{1}H NMR (500 MHz, D_2O): δ = 5.02 (d, $J_{1,2}$ = 8.2 Hz, 1H; H-1), 4.08 (m, 1H; H-5), 3.76 (m, 1H; H-3), 3.70 (dd, $J_{6a,6b}$ = 11.6 Hz, $J_{5,6a}$ = 7.6 Hz, 1H; H-6a), 3.60 (m, 1H; H-2), 3.56 (m, 1H; H-4), 3.46 (m, 3H; H-6b, CH_2N), 3.00 (m, 2H; CH_2NH_2), 1.73 ppm (m, 4H, CH_2); ^{13}C NMR (125.7 MHz, D_2O): δ = 175.7 (CN), 87.4 (C-1), 77.1 (C-4), 75.8 (C-3), 72.8 (C-2), 69.1 (C-5), 50.5 (CH_2N), 41.5 (CH_2NH_2), 32.5 (C-6), 27.9, 26.5 ppm (CH_2); MS (FAB): *m/z* (%): 314 (40) $[M+Na-HCl]^+$, 292 (90); elemental analysis calcd (%) for $C_{11}H_{22}ClN_3O_4S$: C 40.30, H 6.76, N 12.82, S 9.78; found: C 39.95, H 6.47, N 12.49, S 9.41.

5-*N*,6-*S*-[*N*′-(4-Dansylamino)butyliminomethylidene]-6-thionojirimycin (6S-NDI-NJ): Et_3N (64 μL, 0.21 mmol) and 5-dimethylaminonaphtalene-1-sulfonyl chloride (61.8 mg, 1.1 eq) were added to a solution of **4** (68 mg, 0.21 mmol) in anhyd DMF (15 mL) at 0 °C under argon. The mixture was stirred for 4 h, and the solvent was removed under reduced pressure. The resulting residue was purified by column chromatography by using 90:10:1→60:10:1 CH_2Cl_2/MeOH/H_2O to obtain the target fluorescent sp^2-iminosugar 6S-NDI-NJ (107 mg, 98%). R_f = 0.63 (40:10:1 CH_2Cl_2/MeOH/H_2O); $[\alpha]_D$ = −7.4 (*c* = 0.7 in MeOH); ^{1}H NMR (500 MHz, CD_3CN): δ = 8.52 (d, 1H; dansyl), 8.24 (d, 1H; dansyl), 8.15 (d, 1H; dansyl), 7.60 (m, 2H; dansyl), 7.28 (d, 1H; dansyl), 5.48 (d, $J_{1,2}$ = 3.4 Hz, 1H; H-1), 3.79 (m, 1H; H-5), 3.62 (t, $J_{2,3}$ = $J_{3,4}$ = 9.5 Hz, 1H; H-3), 3.46 (dd, $J_{6a,6b}$ = 11.2 Hz, $J_{5,6a}$ = 4.4 Hz, 1H; H-6a), 3.40 (dd, 1H; H-2), 3.30 (t, $J_{4,5}$ = 9.3 Hz, 1H; H-4), 3.10 (dd, $J_{5,6b}$ = 7.3 Hz, 1H; H-6b), 3.06 (t, $^3J_{H,H}$ = 10.5 Hz, 2H; CH_2N), 3.00 (m, 2H, CH_2NH), 2.83 (brs, 6H; dansyl), 1.44 (m, 2H; CH_2), 1.34 ppm (m, 2H; CH_2); ^{13}C NMR (125.7 MHz, CD_3CN): δ = 163.1 (CN), 152.0, 135.4, 130.2–129.5, 129.2, 128.4, 123.7, 119.1, 115.5 (dansyl), 76.3 (C-1), 74.3 (C-4), 72.8 (C-3), 71.5 (C-6), 61.1 (C-5), 54.5 (CH_2N), 44.9 (dansyl), 42.5 (CH_2NH), 31.2 (C-6), 26.8, 26.7 ppm (CH_2); HRMS (FAB): *m/z*: 547.1661 $[M+Na]^+$; elemental analysis calcd (%) for $C_{23}H_{32}N_4O_6S_2$ (547.1661): C 52.65, H 6.15, N 10.68, S 12.22; found: C 52.34, H 6.10, N 10.47, S 11.89.

Cell culture: Human skin fibroblasts were cultured in DMEM/10% FBS at 37 °C in a humidified atmosphere containing 5% CO_2. One control cell line (H37) and three lines of GD cells that carried the β-Glu mutations F213I/F213I, L444P/L444P, and N370S/N370S, respectively were used.[15] The culture medium was replaced every 2 d with fresh media supplemented with or without chaperone at the indicated concentrations.

In vitro neural cell differentiation: The P19 mouse embryonic carcinoma (EC) cells, obtained from ATCC (American Type Culture Collection), were grown in α-minimum essential medium (α-MEM; Gibco BRL, MD, USA) containing 10% of fetal bovine serum and 1% antibiotic-antimycotic ×100 (Gibco BRL) at 37 °C in the presence of 5% CO_2. For the differentiation process, the P19 cells were removed from the culture flask with 0.25% trypsin solution, and 1×10^6 cells were seeded into 10 mL of α-MEM containing 5% fetal calf serum, and 0.6 μM all-*trans* retinoic acid (Sigma).[37,38] Cells were cultured for one or two weeks to get immature and mature neuronal cells.

Immunoblotting: Except otherwise stated, all procedures were carried out at 4 °C. Fibroblasts were lysed by sonication in PBS supplemented with 1% Triton X-100 and a protease inhibitor cocktail (Roche Diagnostics). After a brief centrifugation to remove insoluble material, the supernatant was collected. For the enzyme assay, 4 μL of the precipitates was used as described below. For immunoblotting, supernatant with the same volume of 2× SDS-PAGE sample buffer was heated at 100 °C for 3 min. SDS-PAGE and Western transfer were carried out as previously described.[14,15] The blots were probed with rabbit polyclonal anti-β-glucosidase and mouse monoclonal anti-α-tubulin antibodies (Santa Cruz Biotech, Santa Cruz, CA, USA) and developed by using an ECL kit (GE Healthecare Japan).

In vitro enzyme assay: Lysosomal enzyme activities in cell lysates were determined as described.[39–42] Briefly, cells were scraped into ice-cold H_2O (10^6 mL) and lysed by sonication. Insoluble materials were removed by centrifugation and protein concentrations were determined with a BCA microprotein assay kit (Pierce Biotech, Waltham, MA, USA). The lysate (10 μL) was incubated at 37 °C with the substrate solution (20 μL) in 0.1 M citrate buffer, pH 4.5. The substrates were 4-methylumbelliferone-conjugated α-D-glucopyranoside (for α-glucosidase), α-D-galactopyranoside (for α-galactosidase), β-D-galactopyranoside (for β-galactosidase), and *N*-acetyl-β-D-glucosaminide (for β-hexosaminidase) obtained from Sigma. For

β-Glu, activities in cell lysates were determined by using 4-methylumbelliferone-conjugated β-D-glucopyranoside as a substrate. The lysates 10 μL were incubated at 37 °C with the substrate solution (20 μL) in 0.1 M citrate buffer, pH 5.2, supplemented with sodium taurocholate (0.8% *w/v*). The reactions were terminated by adding 0.2 mL of 0.2 M glycine sodium hydroxide buffer (pH 10.7). The liberated 4-methylumbelliferone was measured with a Perkin–Elmer Luminescence Spectrometer (excitation wave length: 340 nm; emission: 460 nm). One unit of enzyme activity was defined as nmol of 4-methylumbelliferone released per hour and normalized for the amount of protein contained in the lysates (Figure 1).[14,15]

Intact-cell enzyme assay: β-Glu activities in live cells were estimated by the methods described by Sawkar et al.[19] with some modification. Briefly, cells in 96-well assay plates were treated with compounds for 4 d. After washing with PBS, the cells were incubated in PBS (8 μL) and 0.2 M acetate buffer (8 μL; pH 4.0). The reaction was started by addition of 5 mM 4-methylumbelliferyl-β-D-glucoside (10 μL), followed by incubation at 37 °C for 1 h. The reaction was stopped by lysing the cells by the addition of 0.2 M glycine buffer (200 μL; pH 10.7), and the liberated 4-methylumbelliferone was quantified. For neuronal cells, experiments were performed in 35 mm dishes. Every experiment was performed in parallel with cells that had been preincubated with or without conduritol B epoxide (CBE, Toronto Research Chemicals; North York, Ontario, Canada) at 0.5 mM for 1 h. The CBE-sensitive component was ascribed to lysosomal β-Glu, whereas the CBE insensitive component was ascribed to non-lysosomal β-Glu (Figure 2).

Cytotoxicity assay: Cytotoxicity assay was performed by using the colorimetric assay reagent TetraColor One (Seikagaku, Tokyo, Japan),[43] according to the manufacturer's instructions. Cells were seeded on a 96-well assay plate at a density of 3.0×10^4 cells/mL medium and incubated for 4 d with the chaperone. Then, TetraColor One reagent (10 μL) was added to each well, and cells were incubated for another 2 h. The absorbance at 450 nm was measured with a reference wavelength at 630 nm in the microplate reader. Measurement was repeated in triplicate and then averaged for each sample. Results are expressed as mean ± standard deviation (SD).

pH-dependent and heat stability of β-Glu in vitro: Cell lysates were incubated in 0.1 M citrate–phosphate buffer at pH 7 at 37 °C and 48 °C for the time indicated. Incubation was terminated by the addition of 3 volumes of 0.2 M citrate phosphate buffer (pH 5.2), immediately followed by chilling on ice. The enzyme assay was carried out at pH 5.2 as described above (Figure 3).[14]

Measurement of 6S-NDI-NJ release from living fibroblasts: Living GD fibroblasts were incubated with 6S-NDI-NJ in DMEM/10% FBS (30 μL) at 37 °C in 5% CO_2 for 4 d, then the loading solution was replaced with fresh medium after washing twice with DMEM. The cells were cultured for 1–6 d. The medium was aspirated for measurement of the 6S-NDI-NJ concentration. Release of 6S-NDI-NJ from fibroblasts into the surrounding medium was monitored with a Perkin–Elmer Luminescence Spectrometer (excitation wave length: 337 nm; emission: 517 nm) (Figure 4).[44]

Immunofluorescence staining, confocal microscopy and fluorometrical analysis: Fibroblast and neuronal cell lines were grown on glass coverslips in 35 mm dishes. The cells were treated without or with 6S-NDI-NJ (30 μL) at 37 °C in 5% CO_2 for 4 d. Cells were then fixed with 4% formaldehyde for 20 min. After serial washings and permeabilization with 0.1% Triton X-100, rabbit polyclonal anti-glucocerebrosidase antibody (H-300, Santa Cruz, 1:100), rabbit polyclonal anti-calnexin antibody (H70, Santa Cruz, 1:100), mouse monoclonal LAMP-2 antibody (H4B4, Santa Cruz, 1:100), mouse monoclonal anti-β III tubulin antibody (H70, Santa Cruz, 1:100) and rabbit polyclonal anti-MAP2 antibody (H-300, Santa Cruz, 1:100) were applied for 1 h, followed by secondary antibody Alexa Fluor 647 goat anti-rabbit IgG (1:500), Alexa Fluor 647 goat anti-mouse IgG (1:500), Alexa Fluor 546 donkey anti-goat IgG (1:500), Alexa Fluor 546 goat anti-mouse anti-mouse IgG (1:1000) and Alexa Fluor 546 goat anti-rabbit IgG (1:1000) (Invitrogen, Carlsbad, CA, USA). For nuclear staining, cells were incubated with Syto 59 (Invitrogen) for 30 min. Fluorescent images were collected by using a Leica TSC SP2 confocal laser microscope (Leica, Wetzler, Germany).[14,15] For fluorometrical anlysis, fluorescence intensity in randomly selected 25 fields per cells was measured by using an Infinite F500 plate reader (Tecan Japan, Tokyo, Japan; Figures 5 and 6).

Competitive inhibition of 6S-NDI-NJ uptake by glucose in fibroblast: Normal fibroblasts were seeded in 35 mm dishes with coverslips and cultured in DMEM/10% FBS for 2 d. The medium was removed and replaced with 30 μM 6S-NDI-NJ solutions containing 25, 50, and 100 mM glucose (Wako, Tokyo, Japan).[45] After 1 h incubation, cells were washed in PBS (2×) and fixed. Fluorescent images were collected by using confocal laser microscope.

Acknowledgements

This research was supported by grants from the Ministry of Education, Culture, Science, Sports, and Technology of Japan (20390297, 13680918, 14207106), the Ministry of Health, Labour and Welfare of Japan (H14-Kokoro-017, H17-Kokoro-019, H20-Kokoro-022 and a grant for Research for Intractable Diseases), the Spanish Ministerio de Ciencia e Innovación (contract numbers CTQ2006-15515-C02-01/BQU and CTQ2007-61180/PPQ), the Junta de Andalucía (Project P08-FQM-03711), the European Union (FEDER) and the Fundación Ramón Areces. M.A.-M. is a FPU fellow.

Keywords: chaperones · fluorescent probes · Gaucher disease · glucosidases · iminosugars

[1] E. Beutler, G. A. Grabowski in *The Metabolic and Molecular Bases of Inherited Disease*, 8th ed. (Eds.: C. R. Scriver, A. L. Beaudet, W. S. Sly, D. Valle), McGraw-Hill, New York, **2001**, pp. 2641–2670.
[2] T. D. Butters, *Curr. Opin. Chem. Biol.* **2007**, *11*, 412–418.
[3] N. W. Barton, R. O. Brady, J. M. Dambrosia, A. M. Di Bisceglie, S. H. Doppelt, S. C. Hill, H. J. Mankin, G. J. Murray, R. I. Parker, C. E. Argoff, *N. Engl. J. Med.* **1991**, *324*, 1464–1470.
[4] T. Cox, R. Lachmann, C. Hollak, J. Aerts, S. van Weely, M. Hrebicek, F. Platt, T. Butters, R. Dwek, C. Moyses, *Lancet* **2000**, *355*, 1481–1485.
[5] G. A. Grabowski, N. Leslie, R. Wenstrup, *Blood Rev.* **1998**, *12*, 115–133.
[6] F. M. Platt, M. Jeyakumar, U. Andersson, D. A. Priestman, R. A. Dwek, T. D. Butters, *J. Inherited Metab. Dis.* **2001**, *24*, 275–290.
[7] R. Schiffmann, M. P. Heyes, J. M. Aerts, J. M. Dambrosia, M. C. Patterson, T. DeGraba, C. C. Parker, G. C. Zirzow, K. Oliver, G. Tedeschi, *Ann. Neurol.* **1997**, *42*, 613–621.
[8] C. A. Prows, N. Sanchez, C. Daugherty, G. A. Grabowski, *Am. J. Med. Genet.* **1997**, *71*, 16–21.
[9] M. Aoki, Y. Takahashi, Y. Miwa, S. Iida, K. Sukegawa, T. Horai, T. Orii, N. Kondo, *Eur. J. Pediatr.* **2001**, *160*, 63–64.
[10] J. M. F. G. Aerts, C. E. Hollak, R. G. Boot, J. E. Groener, M. Maas, *J. Inherited Metab. Dis.* **2006**, *29*, 449–456.
[11] I. Ron, M. Horowitz, *Hum. Mol. Genet.* **2005**, *14*, 2387–2398.
[12] G. Parenti, *EMBO Mol. Med.* **2009**, *1*, 268–279.

[13] S. Ogawa, M. Ashiura, C. Uchida, S. Watanabe, C. Yamazaki, K. Yamagishi, J. Inokuchi, *Bioorg. Med. Chem. Lett.* **1996**, *6*, 929–932.
[14] H. Lin, Y. Sugimoto, Y. Ohsaki, H. Ninomiya, A. Oka, M. Taniguchi, H. Ida, Y. Eto, S. Ogawa, Y. Matsuzaki, M. Sawa, T. Inoue, K. Higaki, E. Nanba, K. Ohno, Y. Suzuki, *Biochim. Biophys. Acta Mol. Basis Dis.* **2004**, *1689*, 219–228.
[15] K. Lei, H. Ninomiya, M. Suzuki, T. Inoue, M. Sawa, M. Iida, H. Ida, Y. Eto, S. Ogawa, K. Ohno, Y. Suzuki, *Biochim. Biophys. Acta Mol. Basis Dis.* **2007**, *1772*, 587–596.
[16] Z. Luan, L. Li, H. Ninomiya, K. Ohno, S. Ogawa, T. Kubo, M. Iida, Y. Suzuki, *Blood Cells Mol. Dis.* **2010**, *44*, 48–54.
[17] Z. Luan, H. Ninomiya, K. Ohno, S. Ogawa, T. Kubo, M. Iida, Y. Suzuki, *Brain Dev.* **2010**; DOI: doi:10.1016/j.braindev.2009.12.005
[18] A. R. Sawkar, W. C. Cheng, E. Beutler, C. H. Wong, W. E. Balch, J. W. Kelly, *Proc. Natl. Acad. Sci. USA* **2002**, *99*, 15428–15433.
[19] A. R. Sawkar, S. L. Adamski-Werner, W. C. Cheng, C. H. Wong, E. Beutler, K. P. Zimmer, J. W. Kelly, *Chem. Biol.* **2005**, *12*, 1235–1244.
[20] R. A. Steet, S. Chung, B. Wustman, A. Powe, H. Do, S. A. Kornfeld, *Proc. Natl. Acad. Sci. USA* **2006**, *103*, 13813–13818.
[21] P. Compain, O. R. Martin, C. Boucheron, G. Godin, L. Yu, K. Ikeda, N. Asano, *ChemBioChem* **2006**, *7*, 1356–1359.
[22] H. H. Chang, N. Asano, S. Ishii, Y. Ichikawa, J. Q. Fan, *FEBS J.* **2006**, *273*, 4082–4092.
[23] Z. Yu, A. R. Sawkar, *J. Med. Chem.* **2007**, *50*, 94–100.
[24] G. J. Kornhaber, M. B. Tropak, G. H. Maegawa, S. J. Tuske, S. J. Coales, D. J. Mahuran, Y. Hamuro, *ChemBioChem* **2008**, *9*, 2643–2649.
[25] M. B. Tropak, G. J. Kornhaber, B. A. Rigat, G. H. Maegawa, J. D. Buttner, J. E. Blanchard, C. Murphy, S. J. Tuske, S. J. Coales, Y. Hamuro, E. D. Brown, D. J. Mahuran, *ChemBioChem* **2008**, *9*, 2650–2652.
[26] W. Zheng, J. Padia, D. J. Urban, A. Jadhav, O. Goker-Alpan, A. Simeonov, E. Goldin, D. Auld, M. E. LaMarca, J. Inglese, C. P. Austin, E. Sidransky, *Proc. Natl. Acad. Sci. USA* **2007**, *104*, 13192–13197.
[27] M. I. García-Moreno, P. Díaz-Pérez, C. Ortiz Mellet, J. M. García Fernández, *J. Org. Chem.* **2003**, *68*, 8890–8901.
[28] M. Aguilar-Moncayo, T. M. Gloster, J. P. Turkenburg, M. I. García-Moreno, C. Ortiz Mellet, G. J. Davies J. M. García Fernández, *Org. Biomol. Chem.* **2009**, *7*, 2738–2749.
[29] B. Brumshtein, M. Aguilar-Moncayo, M. I. García-Moreno, C. Ortiz Mellet, J. M. García Fernandez, I. Silman, Y. Shaaltiel, D. Aviezer, J. L. Sussman, A. H. Futerman, *ChemBioChem* **2009**, *10*, 1480–1485.
[30] Z. Luan, K. Higaki, M. Aguilar-Moncayo, H. Ninomiya, K. Ohno, M. I. García-Moreno, C. Ortiz Mellet, J. M. García Fernández, Y. Suzuki, *ChemBioChem* **2009**, *10*, 2780–2792.
[31] T. M. Wrodnigg, S. G. Withers, A. E. Stütz, *Bioorg. Med. Chem. Lett.* **2001**, *11*, 1063–1064.
[32] A. Hermetter, H. Scholze, A. E. Stütz, S. G. Withers, T. M. Wrodnigg, *Bioorg. Med. Chem. Lett.* **2001**, *11*, 1339–1342.
[33] M. van Scherpenzeel, R. J. B. H. N. van den Berg, W. E. Donker-Koopman, R. M. J. Liskamp, J. M. F. G. Aerts, H. S. Overkleeft, R. J. Pieters, *Bioorg. Med. Chem.* **2010**, *18*, 267–274.
[34] A. J. Steiner, A. E. Stütz, T. M. Wrodnigg, C. A. Tarling, S. G. Withers, A. Hermetter, H. Schmidinger, *Bioorg. Med. Chem. Lett.* **2008**, *18*, 1922–1925.
[35] K. Fantur, D. Hofer, G. J. Schitter, A. J. Steiner, B. M. Pabst, T. M. Wrodnigg, A. E. Stütz, E. Paschke, *Mol. Genet. Metab.* **2010**, *100*, 262–268.
[36] K. Dax, B. Gaigg, V. Grassberger, B. Kolbringer, A. E. Stütz, *J. Carbohydr. Chem.* **1990**, *9*, 479–499.
[37] E. M. Jones-Villeneuve, M. W. McBurney, K. A. Rogers, V. I. Kalnins, *J. Cell Biol.* **1982**, *94*, 253–262.
[38] E. M. Jones-Villeneuve, M. A. Rudnicki, J. F. Harris, M. W. McBurney, *Mol. Cell. Biol.* **1983**, *3*, 2271–2279.
[39] J. Matsuda, O. Suzuki, A. Oshima, Y. Yamamoto, A. Noguchi, K. Takimoto, M. Itoh, Y. Matsuzaki, Y. Yasuda, S. Ogawa, Y. Sakata, E. Nanba, K. Higaki, Y. Ogawa, L. Tominaga, K. Ohno, H. Iwasaki, H. Watanabe, R. O. Brady, Y. Suzuki, *Proc. Natl. Acad. Sci. USA* **2003**, *100*, 15912–15917.
[40] A. M. Vaccaro, M. Muscillo, M. Tatti, R. Salvioli, E. Gallozzi, K. Suzuki, *Clin. Biochem.* **1987**, *20*, 429–433.
[41] S. Ichisaka, K. Ohno, I. Yuasa, E. Nanba, H. Sakuraba, Y. Suzuki, *Brain Dev.* **1998**, *20*, 302–306.
[42] Y. Suzuki, A. Tsuji, K. Omura, G. Nakamura, S. Awa, M. Kroos, A. J. Reuser, *Clin. Genet.* **1988**, *33*, 376–385.
[43] K. Kawasaki, A. Nishio, H. Nakamura, K. Uchida, T. Fukui, M. Ohana, H. Yoshizawa, S. Ohashi, H. Tamaki, M. Matsuura, M. Asada, T. Nishi, H. Nakase, S. Toyokuni, W. Liu, J. Yodoi, K. Okazaki, T. Chiba, *Lab. Invest.* **2005**, *85*, 1104–1117.
[44] P. L. Tran, M. A. Deugnier, *Carcinogenesis* **1985**, *6*, 433–439.
[45] B. Olgemöller, S. Schwaabe, E. D. Schleicher, K. D. Gerbitz, *Biochim. Biophys. Acta* **1990**, *1052*, 47–52.
[46] A. R. Sawkar, M. Schmitz, K. P. Zimmer, D. Reczek, T. Edmunds, W. E. Balch, J. W. Kelly, *ACS Chem. Biol.* **2006**, *1*, 235–251.
[47] J. Q. Fan, S. Ishii, N. Asano, Y. Suzuki, *Nat. Med.* **1999**, *5*, 112–115.
[48] B. L. Cantarel, P. M. Coutinho, C. Rancurel, T. Bernard, V. Lombard, B. Henrissat, *Nucleic Acid Res.* **2009**, *37*, D233–D238.
[49] M. Egido-Gabás, D. Canals, J. Casas, A. Llebaria, A. Delgado, *ChemMedChem* **2007**, *2*, 992–994.
[50] M. P. Dale, H. Ensley, K. Kern, K. Sastry, L. D. Byers, *Biochemistry* **1985**, *24*, 3530–3539.

Received: June 3, 2010
Published online on November 9, 2010

Journal of Proteomics & Bioinformatics -Open Access

www.omicsonline.com JPB/Vol.3 Issue 4

Research Article OPEN ACCESS Freely available online doi:10.4172/jpb.1000128

Molecular Basis of Chemical Chaperone Effects of *N*-octyl-β-valienamine on Human β-glucosidase in Low/neutral pH Conditions

Hiroyuki Jo[1], Katsuyuki Yugi[1], Seiichiro Ogawa[1], Yoshiyuki Suzuki[2] and Yasubumi Sakakibara[1]*

[1]Department of Biosciences and Informatics, Faculty of Science and Technology, Keio University, 3-14-1 Hiyoshi, Kohoku-ku, Yokohama 223-8522, Japan

[2]International University of Health and Welfare Graduate School, 2600-1 Kita Kanemaru, Otawara 324-8501, Japan

Abstract

Chemical chaperone therapy is a strategy for restoring the activities of mutant lysosomal hydrolases. This therapy involves chemical compounds binding to the dysfunctional enzymes. The chemical chaperones for lysosomal hydrolases are anticipated to stabilize folding of target enzymes by binding at neutral pH and rescuing enzyme activities by dissociation in acidic conditions after transport to lysosome. However, the molecular basis describing the mechanism of action of chemical chaperones has not been analysed sufficiently. Here we present results derived from molecular dynamics simulations showing that the binding free energy between human â-glucosidase and its known chemical chaperone, *N*-octyl-â-valienamine (NOV), is lower at pH 7 than at pH 5. This observation is consistent with the hypothetical activity of chemical chaperones. The pH conditions were represented as differences in the protonation states of ionizable residues which were determined from predicted pKa values. The binding free energy change is negatively correlated to the number of hydrogen bonds (H-bonds) formed between GLU235, the acid/base catalyst of the enzyme, and the N atom of NOV. At pH 7, NOV is inserted further into the active site than at pH 5. Consequently, this provides an increase in the number of H-bonds formed. Thus, we conclude that the dissociation of NOV from â-glucosidase at pH 5 occurs due to an increase in the binding free energy change caused by protonation of several residues which decreases the number of H-bonds formed between NOV and the enzyme.

Keywords: Molecular dynamics; Binding free energy change; Hydrogen bonds; Human â-glucosidase; Chemical chaperone; N-octyl-â-valienamine (NOV); pKa

Introduction

Dysfunctional lysosomal hydrolases activities trigger accumulation of waste products that consequently lead to a variety of severe human diseases. For example, Fabry disease (OMIM: 301500), GM1-gangliosidosis (OMIM: 230500) and Gaucher disease (OMIM: 230800) are caused by deficiencies of â-galactosidase A (Davies et al., 1996; Okumiya et al., 1995a), â-galactosidase(Boustany et al., 1993) and â-glucosidase(Amaral et al., 2000), respectively. In particular, single mutations of â-glucosidase, which catalyzes the cleavage of the â-glucoside bond of sugar chains under acidic conditions in the lysosome, can lead to the accumulation of glucosylceramide (Figure 1A) (Suzuki, 2006; Suzuki, 2008; Suzuki et al., 2007). Although some of these mutant enzymes do not lose their activity completely, the proteins are degraded and hence fail to be transported into the lysosome. As such, the absence of â-glucosidases in the lysosome is considered to be the dominant reason for the accumulation of glycolipids rather than a decrease in catalytic activity of the enzyme.

In (Okumiya et al., 1995) reported that galactose restores mutant á-galactosidase activity (Okumiya et al., 1995b). Subsequently, Fan et al. (1999) discovered a paradoxical phenomenon that 1-deoxygalactonojirimycin, an inhibitor of á-galactosidase A, restores intracellular activity of mutant á-galactosidase A in cultured lymphoblasts from human patients and in transgenic mouse tissues expressing the mutant enzyme (Fan et al., 1999). Furthermore, Lin et al. reported that N-octyl-â-valienamine (NOV, Figure 1B), an inhibitor of â-glucosidase, exhibits similar effects on the intracellular activity of â-glucosidase (Lin et al., 2004).

The molecular mechanism describing how enzyme activity is restored by these inhibitors was proposed as follows:(Matsuda et al., 2003; Yam et al., 2005) (1) mutant enzymes are degraded in the cytoplasm because they are unstable at neutral pH, (2) binding of certain inhibitors in the ER/Golgi compartment provides stabilization of the misfolded mutant enzymes which consequently allows transport of the enzymes to the lysosome without degradation, and (3) dissociation of the inhibitors from the mutant enzymes rescues intra-lysosomal activity, thereby clearing accumulated glycolipids. These inhibitors are termed "chemical chaperones" because they stabilize proteins in a similar manner to chaperone proteins(Leandro and Gomes, 2008; Perlmutter, 2002).

However, there is insufficient information detailing the paradoxical role of the chemical chaperones: the enzyme activity in the lysosome is restored by strong inhibitors. Consequently, the detailed mechanism of action of chemical chaperones remains poorly understood.

***Corresponding author:** Yasubumi Sakakibara, Department of Biosciences and Informatics, Faculty of Science and Technology, Keio University, 3-14-1 Hiyoshi, Kohoku-ku, Yokohama 223-8522, Japan, E-mail: yasu@bio.keio.ac.jp

Received February 10, 2010; **Accepted** March 22, 2010; **Published** March 22, 2010

Citation: Jo H, Yugi K, Ogawa S, Suzuki Y, Sakakibara Y (2010) Molecular Basis of Chemical Chaperone Effects of N-octyl-b-valienamine on Human b-glucosidase in Low/neutral pH Conditions. J Proteomics Bioinform 3: 104-112. doi:10.4172/jpb.1000128

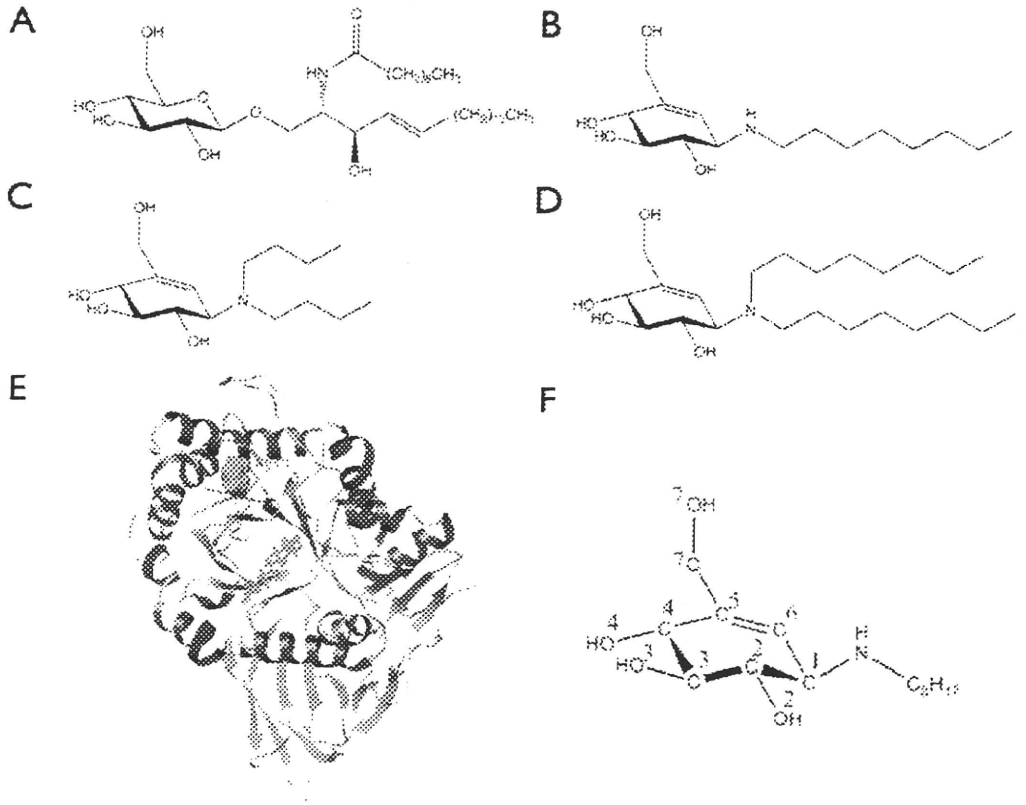

Figure 1: The structures of glycosylceramide and the chemical compounds docked to β-glucosidase in this study. (A) glycosylceramide, (B) N-octyl-β-valienamine (NOV), (C) N,N-dibutyl-β-valienamine (NNBV), (D) N,N-dioctyl-β-valienamine (NNOV), and (E) the complex of NOV (red) and β-glucosidase. Colored in magenta is F213 residue analyzed in later sections. Numbering of atoms of NOV are shown in (F).

Here we show the mechanism of restoring action of NOV on human β-glucosidase using molecular dynamics (MD) simulations. Initially, a plausible conformation of the β-glucosidase-NOV complex was predicted using a docking routine. The conformation was subjected to further structural optimization. The free energy changes of β-glucosidase by binding of NOV were calculated both at pH 5 and 7 using the Molecular Mechanics Poisson-Boltzmann Surface Area (MM/PBSA) method (Swanson et al., 2004) implemented in the AMBER9 package (Case et al., 2006). For the MD simulations, the pH 5 and 7 conditions were modeled by varying the protonation states of ionizable residues estimated by PROPKA (Bas et al., 2008; Li et al., 2005). The ΔG of the complex at pH 5 was calculated to be higher than the ΔG value at pH 7. At pH 7, NOV was found to be inserted deeper into the active pocket cavity than at pH 5. The nitrogen atom in the carbon chain of NOV was found to possibly provide the pH-dependent change in binding affinity. The results are consistent with the hypothesis describing the mechanism of restoring action of the chemical chaperone in which NOV dissociates from the enzyme in the acidic environment of the lysosome.

Materials and Methods

Preparation of structural data

The tertiary structure of NOV was generated using ChemDraw and Chem3D (CambridgeSoft Co.) using the first report of its chemical synthesis (Ogawa et al., 1996). Structure optimization was performed using the MM2 force field in Chem3D. Similarly, the structure of N, N-dibutyl-β-valienamine (NNBV, Figure 1C) was also prepared as a homolog of N, N-dioctyl-β-valienamine (NNOV, Figure 1D). NNOV has been reported to be an inhibitor of β-galactosidase without chemical chaperone activity(Lei et al., 2007; Ogawa et al., 1998). Since an MD simulation of the NNOV-enzyme complex provided a distorted NNOV structure (data not shown), NNBV was employed as an alternative ligand. The atomic composition of NNBV is equivalent to NOV. The optimized structure of NOV was superimposed upon the structure of 5-hydroxymethyl-3,4-dihydroxypiperidine (isofagomine, IFM) in the structure of the human β-glucosidase-IFM complex (PDBID: 2nsx) (Lieberman et al., 2007). Following the superimposition, the conformations of the carbon chains of NOV and NNBV were manually adjusted in the binding site to decrease steric hindrances. These conformations were employed as a complex structure of human β-glucosidase and either NOV or NNBV (Figure 1E).

The ionizable residues were protonated according to the pKa value of each residue predicted by PROPKA (Bas et al., 2008; Li et al., 2005) to represent pH 5 and 7 conditions. For example, an ionizable residue in the pH 5 condition was protonated if the predicted pKa of the residue was larger than 5. Otherwise, the deprotonated form was employed.

Molecular dynamics simulation

The force field for NOV and NNBV was generated using the Antechamber module of the AmberTools software suite using the BCC charge model (Case et al., 2005). The generated force field was employed for subsequent molecular dynamics (MD) simulations of the β-glucosidase-NOV complex in combination with the AMBER99-SB force field (FF99SB) and the General

AMBER force field (GAFF) in the AMBER9 package.

Optimizations and production MD simulations of the complex were conducted using the AMBER9 package. FF99 was employed for the force field of the β-glucosidase enzyme models, whereas the force field for NOV and NNBV was generated from GAFF by the Antechamber module of the AMBER9 package. TIP3P explicit water molecules and counter sodium ions were added to the environment. Distances between the enzyme and edges of the box of the periodic boundary conditions were set at 10 Å. The cutoff distances of the van der Waals interactions were 8 Å. The Particle Mesh Ewald method (Essmann et al., 1995) was employed for electrostatic interactions.

Under these conditions, five steps of MD simulations were performed: (1) energy minimization of water, (2) energy minimization of the whole system, (3) adjustment of the temperature (300 K), (4) adjustment of the pressure (1 atm) and (5) production of 3 ns of MD simulations.

In all MD simulations, the time step was 2 fs and the SHAKE algorithm (Ryckaert et al., 1977) was applied. Production MD was performed in the NPT condition. The temperature and the pressure were maintained at 300 K and 1 atm, respectively.

Calculation of the binding free energy change

The obtained MD trajectory was used to calculate the binding free energy change using the MM/ PBSA method(Swanson et al., 2004) implemented in the AMBER9 package (Case et al., 2006). The representative values of the binding free energy changes shown in "Results" section are averages of those calculated from snapshots obtained every 10ns. In MM/PBSA, the binding free energy change ΔGbind is defined as follows:

$$\Delta Gbind = G^C - G^P - G^L$$

where G^C, G^P and G^L are the free energies of the complex, protein (human β-glucosidase) and ligand, respectively. Each term (denoted G^X below) is calculated using the following formula,

$$G^X = E_{MM} + G_p + G_{np} + TS_{MM}$$

where E_{MM} is the molecular mechanical energy, G_p is the polar part of the solvation free energy calculated with a numerical solution of the Poisson-Bolzmann equation, G_{np} is the non-polar part of the solvation free energy calculated with a linear model dependent on the surface area and TS_{MM} is the solute entropy term. The linear model for G_{np} is defined as the following formula:

$$G_{np} = a\,S + b$$

where S is the solvent-accessible surface area, and a and b are parameters. The default settings of a and b in AMBER9 (a=0.0072, b=0.0) were employed. The contribution from the solute entropy term TS_{MM} was ignored in this study.

Analysis of the complex structure in equilibrium

Several structural characteristics of the docked ligand were evaluated using the equilibrated enzyme-ligand complex structure. In this study, the depth of the docked ligand in the active site and the number of hydrogen bonds (H-bonds) between the enzyme and the ligand were measured. The depth of insertion of the ligand into the active site was measured by the distances between the delta carbon of active residues (GLU235 and GLU340) and seven atoms of NOV. GLU235 and GLU340 have been identified as the acid/base catalyst and the nucleophile, respectively (Fabrega et al., 2000; Miao et al., 1994; Premkumar et al., 2005). The formation of an H-bond between the donor and acceptor atoms was judged to exist when the distance between the donor-acceptor pair was ≤ 3.0 Å and the H-bond dihedral angle was ≥ 120¡Æ for at least 20% occupancy of the total simulation period. The criterion of occupancy was determined after examining previous works considering stability of H-bonds using MD simulations, for example a study presenting 50 ps of H-bond duration as the stability criterion(Kieseritzky et al., 2006) and another one which termed less than 10% occupancy as weak H-bonds (Rodziewicz-Motowidlo et al., 2006). In this study, we adopted 20% occupancy as the criterion of H-bond because it was appropriate to exclude trivial donor-acceptor pairs, which emerge when comparatively looser criteria such as 50 ps of duration are employed.

Protonation and conformation of NOV

Further MD simulations were performed on three structural states of NOV whose nitrogen atoms were in different protonation states (Figure 2). This approach was used to evaluate the binding free energy contribution of the H-bond between GLU235

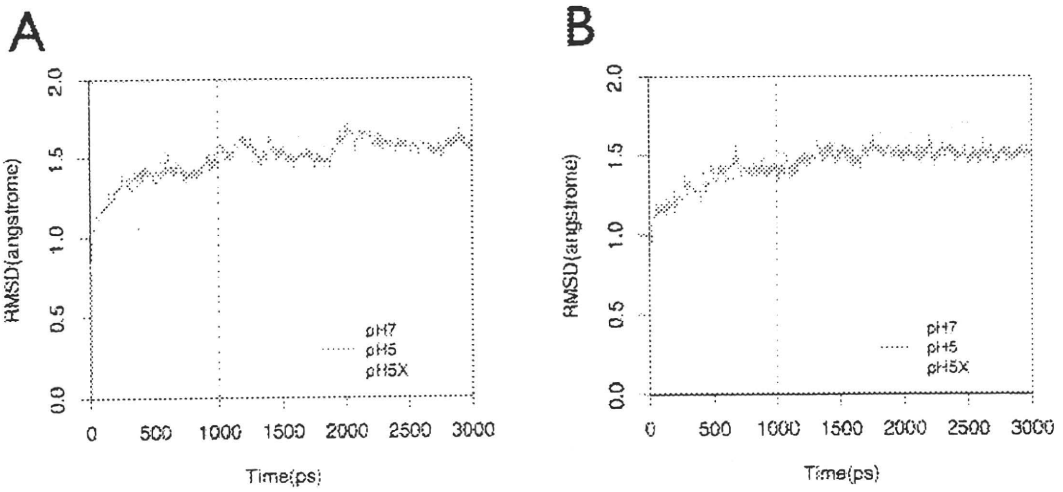

Figure 2: The three possible protonation states of the nitrogen atom of NOV in solvent. (A) The R configuration. (B) the S configuration and (C) the protonated state.

and the N atom of NOV. This additional experiment was motivated by (1) The N atom of NOV corresponds to the glycosyl oxygen atom of glucosylceramide with which GLU235 forms an H-bond during the hydrolytic cleavage process of β-glucosidase, and (2) the equilibrium conformation of NOV indicates a correlation between the number of H-bonds on the N atom of NOV and the binding free energy change (See "Results" for details). With respect to the N atom of NOV, three conformations are possible in the solvent: *R*- (Figure 2A) and S-conformations (Figure2B), the lone-pair electron orbitals being oriented *syn* and *gauche* to the cyclohexene rings, respectively, and the protonated conformation (Figure 2C). The protonated structure of NOV is abbreviated NOV (P) throughout this paper. These three conformations were subjected to MD simulations and energy calculations by MM/PBSA to evaluate the correlation between the binding free energy change and an H-bond connecting the N atom of NOV and GLU235.

Analysis of F213I mutant structure

Effects of NOV on the mutant β-glucosidase were analyzed using the F213I mutation (See Figure 1E for the location of F213 residue). F213I is one of the mutations on which NOV exhibits significant diagnostic effects (Lin et al., 2004). The single residue mutation was incorporated in the wild-type structure using the UCSF Chimera (Pettersen et al., 2004). Protonation was performed according to a prediction result of PROPKA. MD simulations and energy calculations were conducted on the obtained structure of the F213I mutant complex using the same procedures presented above.

Results

Protonation

The predicted pKa values by PROPKA provided protonation of ionizable residues at pH 5 and 7. With respect to aspartic acid, glutamic acid and histidine residues, 14 residues and 4 residues were protonated at pH 5 and 7, respectively (Table 1). The prediction suggested deprotonation of the proton donor GLU235 and protonation of the nucleophilic group GLU340.

Residue	pKa	pH7	pH5
ASP127	5.7	-	+
ASP380	7.14	+	+
GLU233	9.28	+	+
GLU340	5.24	-	+
GLU481	5.06	-	+
HIS60	6.25	-	+
HIS145	6.5	-	+
HIS162	7.34	+	+
HIS223	6.43	-	+
HIS274	6.43	-	+
HIS290	6.43	-	+
HIS328	6.43	-	+
HIS311	7.49	+	+
HIS495	6.5	-	+
NOV	8.69	+	+

Table 1: Predicted pKa values and protonation states of ionizble residues and NOV (+: protonated). Aspartic acid, glutamic acid and histidine residues which are protonated at pH 5 are shown.

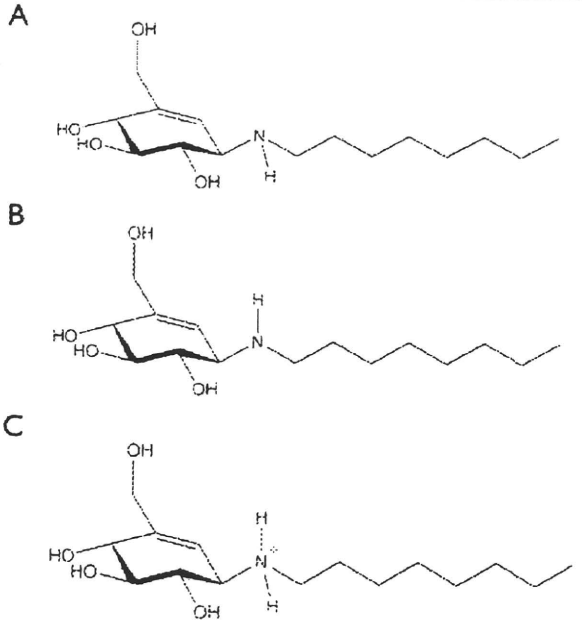

Figure 3: RMSD of the production MD of (A) the β-glucosidase-NOV complex and (B) the enzyme-NNBV complex at equilibrium. The trajectories over the period of 1-3 ns were employed to calculate the binding free energy changes.

Since this prediction contradicts generally considered protonation states of active residues, another structure was prepared in which GLU235 was deprotonated and GLU340 was protonated. This structure is termed "pH 5X", whereas the other structures reflecting the PROPKA predictions are called "pH 7" and "pH 5". The protonation state of pH 5X is same as pH 5 except for GLU235 and GLU340. Regardless of the protonation state of residues in the pH 5 or 5X structures, the proton donor residue was deprotonated at pH 7.

MD simulations and energy calculations

Structural optimization and subsequent MD simulations were performed on six complexes: three structures (pH 7, 5 and 5X) bound by either NOV or NNBV. The RMSDs of the complexes reached a plateau after 1 ns of simulations (Figure 3).

The obtained structures demonstrated that NOV inserts more deeply into the active site of β-glucosidase at pH 7 than at either pH 5 or 5X (Figure 4A). This was corroborated by the distances between delta carbon atoms of the active residues and the C1-6 atoms of NOV (Table 2). Figure 1F provides the nomenclature of the constituent atoms of NOV.

Due to the different binding depths, particular differences were observed in the H-bonds between NOV and the two residues, ASP127 and GLU235. At pH 7, ASP127 formed two stable H-bonds (occupancy > 99%) with NOV via the two oxygen atoms O4 and O5 (Figure 4B and Table 3), whereas H-bonds were formed between ASP127 and other oxygen atoms, O3 and O4, at pH 5 and 5X (Figure 4C and D, respectively). The two oxygen atoms of the GLU235 side-chain formed Hbonds with the nitrogen atom of NOV at pH 7 (Figure 4B and Table 3). At pH 5 and 5X, only one H-bond was observed between GLU235 and the N atom (Figure 4C, D and Table 3). GLU235 was found to form a second H-bond with the O2 atom of NOV at pH 5 (Table 3 and Table 4).

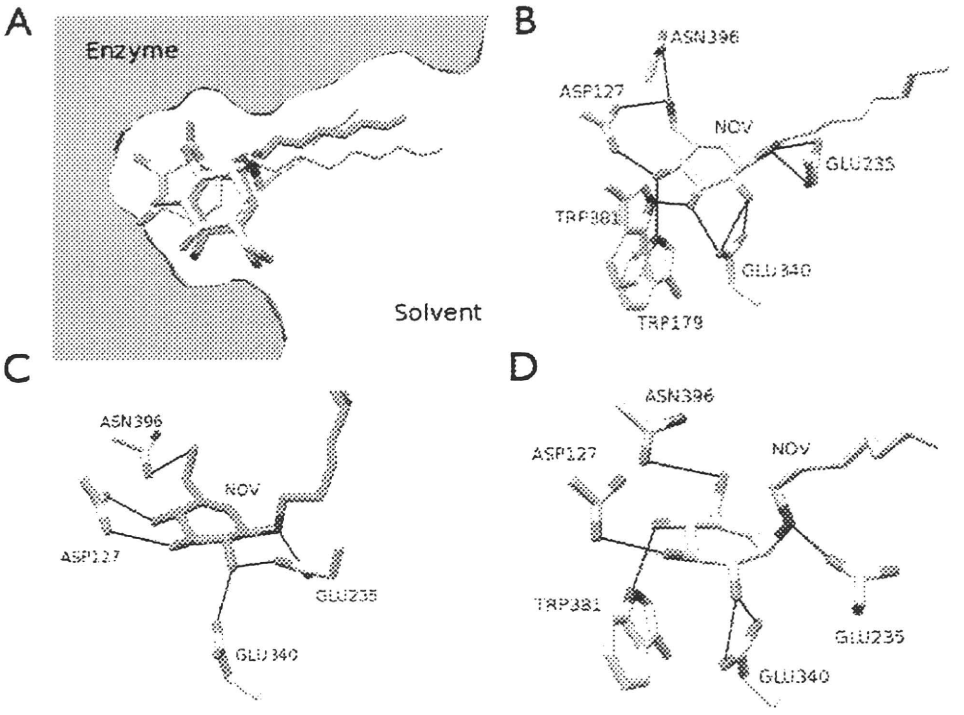

Figure 4: Configurations of NOV bound in the active site. (A) Superposed average structures of NOV (cyan: pH 7, magenta: pH 5, yellow: pH 5X). The enzyme structure is the average structure of β-glucosidase at pH 7. (B?D) H-bonds between the enzyme and NOV at pH 7, 5 and 5X, respectively.

Atom1	Atom2	Distance		
		pH7	pH5	pH5X
GLU235 CD	NOV N	3.182±0.104	3.309±0.135	3.814±0.125
GLU235 CD	NOV C1	4.118±0.133	4.152±0.109	4.694±0.166
GLU235 CD	NOV C2	3.786±0.176	3.986±0.149	4.954±0.214
GLU235 CD	NOV C3	5.357±0.187	5.432±0.153	6.436±0.206
GLU235 CD	NOV C4	6.254±0.193	6.494±0.174	7.362±0.206
GLU235 CD	NOV C5	6.226±0.169	6.440±0.114	7.167±0.165
GLU235 CD	NOV C6	5.364±0.143	5.505±0.105	6.067±0.160
GLU340 CD	NOV N	5.430±0.197	6.152±0.248	5.461±0.240
GLU340 CD	NOV C1	4.486±0.174	5.478±0.258	4.388±0.241
GLU340 CD	NOV C2	3.947±0.114	4.768±0.209	4.095±0.154
GLU340 CD	NOV C3	3.691±0.144	4.837±0.305	4.092±0.200
GLU340 CD	NOV C4	5.119±0.151	6.301±0.327	5.412±0.211
GLU340 CD	NOV C5	5.760±0.166	7.021±0.318	5.626±0.320
GLU340 CD	NOV C6	5.516±0.185	6.697±0.298	5.211±0.354

Table 2: Interatomic distances of NOV and the active site residues at three different pH values (mean ± S.D. Å). The distances at pH 7 were measured to be smaller than at the lower pH values reflecting deeper insertion of the ligand in Figure 4A. See Figure 1F for the nomenclature of the constituent atoms of NOV.

The binding free energy change between β-glucosidase and NOV at pH 7 was lower than the values calculated at pH 5 and 5X. In contrast, NNBV's binding free energy change at pH 7 was almost unchanged in comparison with the values at pH 5, and was higher than the value at pH 5X (Table 5). The binding free energy changes of β-glucosidase and NOV (P) were ΔG = ?46.26 kcal/mol at pH 7, -14.46 kcal/mol at pH 5 and -9.62 kcal/mol at pH 5X. The energy calculations by the MM/PBSA module in AMBER9 were conducted using a trajectory of 1.0-3.0 ns.

Protonation of NOV, hydrogen bond and binding free energy change

We then focused on the correlation between the binding free energy changes and the number of Hbonds between GLU235 and the N atom of NOV. Three different protonated structures of NOV (R, S and P) were prepared to vary the number of possible H-bonds formed (see Materials and Methods). The predicted pKa value of NOV (pKa = 8.69) suggested that NOV (P) is the dominant conformation in solution. The production MD simulations of the three NOV configurations reached equilibrium by 1 ns. Two H-bonds between GLU235 and the N atom were formed in the case of NOV (P) at pH 7 (Table 4 and Figure 5A). The other conditions showed the formation of only one H-bond (Figure 5B and C).

An approximate correlation was observed between the binding free energy change and the number of H-bonds between GLU235 and the N atom of NOV. NOV (P) at pH 7 exhibited the lowest binding free energy change of ΔG = ?46.26 kcal/mol among all nine combinations, three configurations of NOV(R, S and P) and three differently protonated enzymes (Table 5). All three configurations exhibited an increase in the binding free energy change at pH 5. In particular, NOV(P) exhibited the larg-

Atom(NOV)	pH7			Angle(degree)
	Residue	Occupancy (%)	Distance(Å)	
N	GLU235	22.2	2.761±0.10	48.77±9.29
N	GLU235	86.05	2.826±0.09	17.34±10.25
O2	GLU340	21.6	2.893±0.08	48.17±9.00
O2	GLU340	99.9	2.567±0.08	14.74±8.77
O3	TRP179	31.9	2.906±0.06	33.89±8.89
O3	GLU340	55.6	2.813±0.11	16.96±7.82
O4	TRP381	41.75	2.895±0.07	35.60±10.46
O4	ASP127	99.35	2.642±0.10	13.03±7.19
O5	ASN396	35.95	2.890±0.07	20.65±12.66
O5	ASP127	99.15	2.596±0.09	15.96±8.90
Atom(NOV)	pH5			
	Residue	Occupancy (%)	Distance(Å)	Angle(degree)
N	GLU235	94.55	2.796±0.08	15.24±7.96
O2	GLU340	89.15	2.747±0.10	33.25±12.33
O2	GLU235	100	2.533±0.07	11.92±6.51
O3	ASP127	27.3	2.798±0.11	16.17±9.41
O3	ASP127	47.7	2.798±0.11	23.04±11.68
O4	ASP127	65.45	2.721±0.10	14.85±8.39
O4	ASN396	26.75	2.691±0.11	16.17±9.42
O5	ASN396	16.15	2.715±0.12	19.36±11.51
Atom(NOV)	pH5X			
	Residue	Occupancy (%)	Distance(Å)	Angle(degree)
N	GLU235	95.25	2.793±0.09	17.61±9.07
O2	GLU340	24.1	2.833±0.13	35.79±14.04
O2	GLU340	93.85	2.639±0.11	18.34±10.24
O3	ASP127	86.15	2.757±0.11	14.20±7.83
O4	TRP381	34.35	2.896±0.07	32.78±11.49
O4	ASN396	96.796.7	2.704±0.11	17.69±9.14
O5	ASN396	49.85	2.886±0.07	21.07±10.67

Table 3: Distances and angles between the atoms of NOV and the active residues considered to form H-bonds (mean ± S.D. Å and degree, respectively). Occupancy percentage is the duration of a H-bond over simulation time. The atom-residue pairs of occupancy > 10% are presented here.

Protonation	Ligand	H-bond of NOV-GLU235		ΔG
		Possible	Observed	
pH7	NOV(P)	2	2	-46.26
pH7	NOV(R)	1	1	-24.31
pH7	NOV(S)	1	1	-27.01
pH5X	NOV(P)	1	1	-9.62
pH5X	NOV(R)	2	1	-13.45
pH5X	NOV(S)	2	1	-21.73

Table 4: Number of H-bonds formed between GLU235 and the nitrogen atom of NOV. NOV(P) at pH 7 provided two H-bonds (see also Figure 5A) and the lowest binding free energy change (kcal/mol).

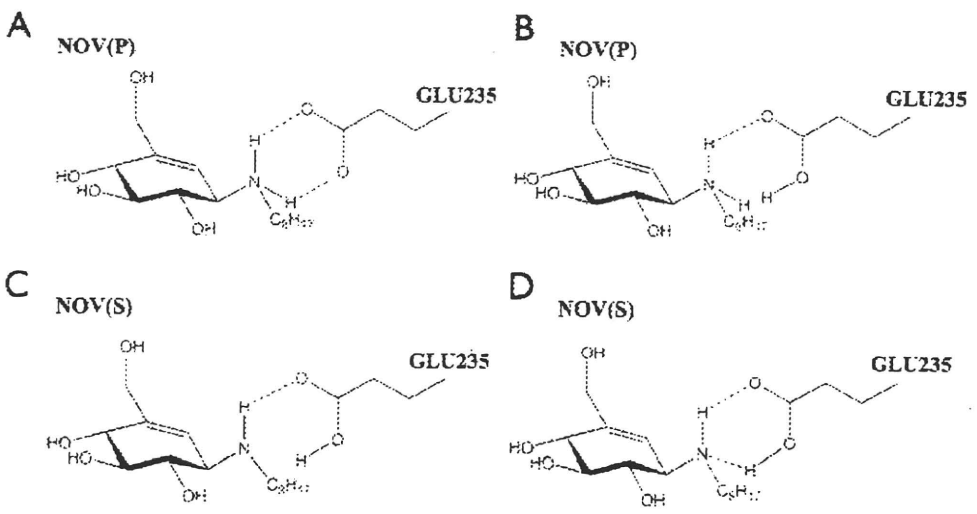

Figure 5: Possible H-bonds between NOVs and the GLU235 residue. (A) Two H-bonds are formed on NOV(P) at pH 7, whereas only one H-bond is formed on NOV(P) at pH 5X (B) and on NOV(S) at pH 7 (C). (D) NOV(S) at pH 5X can provide two H-bonds.

Protonation	Ligand	G_C	G_R	G_L	ΔG	$\Delta\Delta G$
pH7	NNBV	-9789.57	-9830.74	56.88	-15.72	-
pH5	NNBV	-9623.12	-9660.33	51.67	-14.46	1.26
pH5X	NNBV	-9641.08	-9668.93	51.64	-23.79	-8.07
pH7	NOV(P)	-9806.97	-9808.45	47.73	-46.26	-
pH5	NOV(P)	-9619.59	-9652.92	47.8	-14.46	31.8
pH5X	NOV(P)	-9595.54	-9633.78	47.86	-9.62	36.64
pH7	NOV(R)	-9829.37	-9852.35	50	-27.01	-
pH5	NOV(R)	-9680.33	-9712.39	45.51	-13.45	13.56
pH5X	NOV(R)	-9661.72	-9687.94	45.82	-19.61	7.4
pH7	NOV(S)	-9846.67	-9869.74	47.37	-24.31	-
pH5	NOV(S)	-9656.28	-9679.67	40.21	-16.81	7.5
pH5X	NOV(S)	-9647.41	-9667.32	41.64	-21.73	2.58

Table 5: Binding free energy changes of β-glucosidase and three configurations of NOV in three different protonation states (kcal/mol).

est increase in the binding free energy change (i.e. $\Delta\Delta G = 36.64$ kcal/mol) among the three configurations/combinations of NOV (Table 5).

F213I

According to the prediction by PROPKA, the resultant protonation state of the protein including F213I mutation was identical to the wild-type enzyme. The energy calculation showed that the binding free energy change at pH 7 (ΔG = ?38.44 kcal/mol) was lower than at pH 5 and 5X (ΔG = -17.36 kcal/mol and -12.14 kcal/mol, respectively).

Discussion

The MD simulations presented herein theoretically corroborated the hypothetical mechanism of a chemical chaperone. The binding free energy change between β-glucosidase and NOV was demonstrated to increase at pH 5. This is in agreement with the proposed mechanism for a chemical chaperone that dissociates from the target protein in the lysosome and leads to the recovery of enzyme activity (Suzuki, 2008). It was suggested that the binding of a natural substrate/inhibitor homolog NNBV and the enzyme is almost unchanged or rather tighter at pH 5 than at pH 7. This result does not contradict previous studies on NNOV that showed that NNOV does not function as a chemical chaperone (Lei et al., 2007) but inhibits lysosomal activity (Ogawa et al., 1998). These affinity changes are due to a decrease in the number of H-bonds between the enzyme and NOV primarily caused by the protonation states of the residues ASP127 and GLU235. It has been broadly reported that protonation of a few residues can trigger drastic shifts of the pKa or pH optima of enzymes (Brandsdal et al., 2006; Joshi et al., 2000).

The protonation states of the active residues are influential in the configuration of NOV. Since ASP127 is deprotonated only at pH 7, the hydroxyl groups of NOV show no repulsion towards ASP127 due to unfavorable electrostatic forces. Therefore, deprotonated ASP127 allows deeper binding of NOV into the active site than at pH 5 and 5X. The deeper binding leads to the formation of additional H-bonds between NOV and the enzyme. In particular, the number of the H-bonds between the nucleophile GLU235 and the N atom of NOV were presented to be in correlation with the binding free energy changes. If a ligand of β-glucosidase has an oxygen atom at the position of the N atom, such as glucosylceramide, the O atom can form a H-bond with GLU235 at pH 5X but not at pH 7. Since the O atom is not capable of being protonated, the H-bond can be formed only when GLU235 is protonated i.e. pH 5X in this study. At pH 7, the H-bond cannot be formed because neither GLU235 nor the O atom are protonated. Based on the correlation between the binding free energy changes and the number of H-bonds (Table 4), it is anticipated that the complex of the enzyme and such a ligand without the N atom may exhibit a lower binding free energy change at pH 5X than calculated at pH 7. Namely, the ligand without the aforementioned N atom does not show an affinity decrease in acidic conditions which is required if the ligand is to function as a chemical chaperone. This suggests that the position of the N atom is presumably a crucial factor for NOV to acquire chemical chaperone activity towards β-glucosidase The relative decrease of enzyme-NOV affinity at pH 5 was observed for the F213I mutant and the wild-type structure. The predicted pKa value of each residue in the F213I mutant was calculated to be very similar to the pKa values of the residues of the wild-type protein. The binding free energy changes at pH 5 and 5X were higher than at pH 7. Therefore, we conclude that the mechanism of action of NOV upon the F213I mutant is almost identical to that of the wild-type protein. This result is in agreement with a previous biochemical study (Lin et al., 2004).

The strategy used here is applicable to other mutations, chaperones and other glycosidases. Although not examined, there are several single-residue mutations of human β-glucosidase, including L444P and N370S. Among these mutants, the enzymatic activity of the L444P mutation is not significantly restored in the presence of NOV (Lin et al, 2004). In addition, the chemical compound N-(n-nonyl) deoxynojirimycin (NN-DNJ) has been shown to increase the activity of the N370S mutant enzyme(Sawkar et al, 2002). Further studies are required to elucidate why NOV does not function as a chemical chaperone with the β-glucosidase L444P mutant. The mechanism of NN-DNJ in rescuing the activity loss caused by the N370S mutation also requires further studies. Apart from β-glucosidase, human α-galactosidase is a feasible target to examine its interaction mechanism with a known chemical chaperone 1-deoxygalactonojirimycin. This is because the 3D structure, detailed kinetic properties and structural stability of several mutants are available for this enzyme(Fan & Ishii, 2007; Garman & Garboczi, 2004; Ishii et al, 2007). We believe that this study presents a MD simulation strategy for understanding the mechanisms of action of chemical chaperones on lysosomal storage diseases.

Although we have described the action mechanism of a chemical chaperone which binds to an enzyme at pH 7 and dissociates at pH 5, there remains a number of questions to answer, including how chemical chaperones improve protein folding stability during the transport process. To fully understand the roles of

chemical chaperones from the ER to the lysosome, molecular mechanisms of folding stabilization during transport requires further investigation. Recently, several approaches have been proposed to extract 'collective dynamics' or 'essential dynamics' of proteins from MD trajectories using principal component analysis (Berendsen and Hayward, 2000; Kitao and Go, 1999). Such approaches have been employed to evaluate folding stability (Creveld et al., 1998; Kazmirski et al., 1999). It is noteworthy to apply the collective approaches to glycosidases to elucidate how the chemical chaperones stabilize folding of the enzymes during the transport process, which consequently rescues the enzymes from degradation prior to localization in lysosomes.

In conclusion, the MD simulations results strongly support that residue protonation states at low pH values force dissociation of NOV from the β-glucosidase in the lysosome. Consequently, the hypothesis describing the mechanism of action of NOV was theoretically corroborated.

Acknowledgments

This research was supported by grants from the Ministry of Health, Labour and Welfare of Japan (H14-Kokoro-General-016, H17-Kokoro-General-019, H20-Kokoro-General-022) and a Grant program for bioinformatics research and development of the Japan Science and Technology Agency. Part of the MD calculations was performed using the Research Center for Computational Science, Okazaki, Japan.

References

1. Amaral O, Marcao A, Sa Miranda M, Desnick RJ, Grace ME (2000) Gaucher disease: expression and characterization of mild and severe acid β-glucosidase mutations in Portuguese type 1 patients. Eur J Hum Genet 8: 95-102. - CrossRef - PubMed - Google Scholar

2. Bas DC, Rogers DM, Jensen JH (2008) Very fast prediction and rationalization of pKa values for protein-ligand complexes. Proteins 73: 765-783. - CrossRef - PubMed - Google Scholar

3. Berendsen HJ, Hayward S (2000) Collective protein dynamics in relation to function. Curr Opin Struct Biol 10: 165-169. - CrossRef - PubMed - Google Scholar

4. Boustany RM, Qian WH, Suzuki K (1993) Mutations in acid β-galactosidase cause GM1-gangliosidosis in American patients. Am J Hum Genet 53: 881-888. - CrossRef - PubMed - Google Scholar

5. Brandsdal BO, Smalas AO, Aqvist J (2006) Free energy calculations show that acidic P1 variants undergo large pKa shifts upon binding to trypsin. Proteins 64: 740-748. - CrossRef - PubMed - Google Scholar

6. Case DA, Cheatham TE 3rd, Darden T, Gohlke H, Luo R, et al. (2005) The Amber biomolecular simulation programs. J Comput Chem 26: 1668-1688. - CrossRef - PubMed - Google Scholar

7. Case DA, Darden TA, Cheatham TE III, Simmerling CL, Wang J, et al. (2006) AMBER 9: University of California, San Francisco. - CrossRef - PubMed - Google Scholar

8. Creveld LD, Amadei A, van Schaik RC, Pepermans HA, de Vlieg J, et al. (1998) Identification of functional and unfolding motions of cutinase as obtained from molecular dynamics computer simulations. Proteins 33: 253-264. - CrossRef - PubMed - Google Scholar

9. Davies JP, Eng CM, Hill JA, Malcolm S, MacDermot K, et al. (1996) Fabry disease: fourteen α-galactosidase A mutations in unrelated families from the United Kingdom and other European countries. Eur J Hum Genet 4: 219-224. - CrossRef - PubMed - Google Scholar

10. Essmann U, Perera L, Berkowitz ML, Darden T, Lee H, et al. (1995) A Smooth Particle Mesh Ewald Method. J Chem Phys 103: 8577-8593. - CrossRef - PubMed - Google Scholar

11. Fabrega S, Durand P, Codogno P, Bauvy C, Delomenie C, et al. (2000) Human glucocerebrosidase: heterologous expression of active site mutants in murine null cells. Glycobiology 10: 1217-1224. - CrossRef - PubMed - Google Scholar

12. Fan JQ, Ishii S (2007) Active-site-specific chaperone therapy for Fabry disease. Yin and Yang of enzyme inhibitors. FEBS J 274: 4962-4971. - CrossRef - PubMed - Google Scholar

13. Fan JQ, Ishii S, Asano N, Suzuki Y (1999) Accelerated transport and maturation of lysosomal α-galactosidase A in Fabry lymphoblasts by an enzyme inhibitor. Nat Med 5: 112-115. - CrossRef - PubMed - Google Scholar

14. Garman SC, Garboczi DN (2004) The molecular defect leading to Fabry disease: structure of human α-galactosidase. J Mol Biol 337: 319-335. - CrossRef - PubMed - Google Scholar

15. Ishii S, Chang HH, Kawasaki K, Yasuda K, Wu HL, et al. (2007) Mutant α-galactosidase A enzymes identified in Fabry disease patients with residual enzyme activity: biochemical characterization and restoration of normal intracellular processing by 1-deoxygalactonojirimycin. Biochem J 406: 285-295. - CrossRef - PubMed - Google Scholar

16. Joshi MD, Sidhu G, Pot I, Brayer GD, Withers SG, et al. (2000) Hydrogen bonding and catalysis: a novel explanation for how a single amino acid substitution can change the pH optimum of a glycosidase. J Mol Biol 299: 255-279. - CrossRef - PubMed - Google Scholar

17. Kazmirski SL, Li A, Daggett V (1999) Analysis methods for comparison of multiple molecular dynamics trajectories: applications to protein unfolding pathways and denatured ensembles. J Mol Biol 290: 283-304. - CrossRef - PubMed - Google Scholar

18. Kieseritzky G, Morra G, Knapp EW (2006) Stability and fluctuations of amide hydrogen bonds in a bacterial cytochrome c: a molecular dynamics study. J Biol Inorg Chem 11: 26-40. - CrossRef - PubMed - Google Scholar

19. Kitao A, Go N (1999) Investigating protein dynamics in collective coordinate space. Curr Opin Struct Biol 9: 164-169. - CrossRef - PubMed - Google Scholar

20. Leandro P, Gomes CM (2008) Protein misfolding in conformational disorders: rescue of folding defects and chemical chaperoning. Mini Rev Med Chem 8: 901-911. - CrossRef - PubMed - Google Scholar

21. Lei K, Ninomiya H, Suzuki M, Inoue T, Sawa M, et al. (2007) Enzyme enhancement activity of N-octyl-β-valienamine on β-glucosidase mutants associated with Gaucher disease. Biochim Biophys Acta 1772: 587-596. - CrossRef - PubMed - Google Scholar

22. Li H, Robertson AD, Jensen JH (2005) Very fast empirical prediction and rationalization of protein pKa values. Proteins 61: 704-721. - CrossRef - PubMed - Google Scholar

23. Lieberman RL, Wustman BA, Huertas P, Powe AC Jr, Pine CW, et al. (2007) Structure of acid β-glucosidase with pharmacological chaperone provides insight into Gaucher disease. Nat Chem Biol 3: 101-107. - CrossRef - PubMed - Google Scholar

24. Lin H, Sugimoto Y, Ohsaki Y, Ninomiya H, Oka A, et al. (2004) N-octyl-β-valienamine up-regulates activity of F213I mutant beta-glucosidase in cultured cells: a potential chemical chaperone therapy for Gaucher disease. Biochim Biophys Acta 1689: 219-228. - CrossRef - PubMed - Google Scholar

25. Matsuda J, Suzuki O, Oshima A, Yamamoto Y, Noguchi A, et al. (2003) Chemical chaperone therapy for brain pathology in GM1-gangliosidosis. Proc Natl Acad Sci USA 100: 15912-15917. - CrossRef - PubMed - Google Scholar

26. Miao S, McCarter JD, Grace ME, Grabowski GA, Aebersold R, et al. (1994) Identification of Glu340 as the active-site nucleophile in human glucocerebrosidase by use of electrospray tandem mass spectrometry. J Biol Chem 269: 10975-10978. - CrossRef - PubMed - Google Scholar

27. Ogawa S, Ashiura M, Uchida C, Watanabe S, Yamazaki C, et al. (1996) Synthesis of potent β-D-glucocerebrosidase inhibitors: N-alkyl-β-valienamines. Bioorg Med Chem Lett 6: 929-932. - CrossRef - PubMed - Google Scholar

28. Ogawa S, Kobayashi Y, Kabayama K, Jimbo M, Inokuchi J (1998) Chemical modification of betaglucocerebrosidase inhibitor N-octyl-beta-valienamine: synthesis and biological evaluation of N-alkanoyl and N-alkyl derivatives. Bioorg Med Chem 6: 1955-1962. - CrossRef - PubMed - Google Scholar

29. Okumiya T, Ishii S, Kase R, Kamei S, Sakuraba H, et al. (1995a) α-galactosidase gene mutations in Fabry disease: heterogeneous expressions of mutant enzyme proteins. Hum Genet 95: 557-561. - CrossRef - PubMed - Google Scholar

30. Okumiya T, Ishii S, Takenaka T, Kase R, Kamei S, et al. (1995b) Galactose stabilizes various missense mutants of α-galactosidase in Fabry disease. Biochem Biophys Res Commun 214: 1219-1224. - CrossRef - PubMed - Google Scholar

31. Perlmutter DH (2002) Chemical chaperones: a pharmacological strategy for disorders of protein folding and trafficking. Pediatr Res 52: 832-836. - CrossRef - PubMed - Google Scholar

32. Pettersen EF, Goddard TD, Huang CC, Couch GS, Greenblatt DM, et al. (2004) UCSF Chimera—a visualization system for exploratory research and analysis. J Comput Chem 25: 1605-1612. - CrossRef - PubMed - Google Scholar

33. Premkumar L, Sawkar AR, Boldin-Adamsky S, Toker L, Silman I, et al. (2005) X-ray structure of human acid-β-glucosidase covalently bound to conduritol-B-epoxide. Implications for Gaucher disease. J Biol Chem 280: 23815-23819. - CrossRef - PubMed - Google Scholar

34. Rodziewicz-Motowidlo S, Wahlbom M, Wang X, Lagiewka J, Janowski R, et al. (2006) Checking the conformational stability of cystatin C and its L68Q variant by molecular dynamics studies: why is the L68Q variant amyloidogenic? J Struct Biol 154: 68-78. - CrossRef - PubMed - Google Scholar

35. Ryckaert JP, Ciccotti G, Berendsen HJC (1977) Numerical integration of the cartesian equations of motion of a system with constraints: molecular dynamics of n-alkanes. J Comput Phys 23: 327-341. - CrossRef - PubMed - Google Scholar

36. Sawkar AR, Cheng WC, Beutler E, Wong CH, Balch WE, et al. (2002) Chemical chaperones increase the cellular activity of N370S beta-glucosidase: a therapeutic strategy for Gaucher disease. Proc Natl Acad Sci USA 99: 15428-15433. - CrossRef - PubMed - Google Scholar

37. Suzuki Y (2006) β-galactosidase deficiency: an approach to chaperone therapy. J Inherit Metab Dis 29: 471-476. - CrossRef - PubMed - Google Scholar

38. Suzuki Y (2008) Chemical chaperone therapy for GM1-gangliosidosis. Cell Mol Life Sci 65: 351-353. - CrossRef - PubMed - Google Scholar

39. Suzuki Y, Ichinomiya S, Kurosawa M, Ohkubo M, Watanabe H, et al. (2007) Chemical chaperone therapy: clinical effect in murine GM1-gangliosidosis. Ann Neurol 62: 671-675. - CrossRef - PubMed - Google Scholar

40. Swanson JM, Henchman RH, McCammon JA (2004) Revisiting free energy calculations: a theoretical connection to MM/PBSA and direct calculation of the association free energy. Biophys J 86: 67-74. - CrossRef - PubMed - Google Scholar

41. Yam GH, Zuber C, Roth J (2005) A synthetic chaperone corrects the trafficking defect and disease phenotype in a protein misfolding disorder. FASEB J 19: 12-18. - CrossRef - PubMed - Google Scholar

Molecular Genetics and Metabolism 101 (2010) 364–369

Contents lists available at ScienceDirect

Molecular Genetics and Metabolism

journal homepage: www.elsevier.com/locate/ymgme

Chemical chaperone therapy: Luciferase assay for screening of β-galactosidase mutations

Linjing Li [a,b], Katsumi Higaki [a,*], Haruaki Ninomiya [c], Zhuo Luan [b], Masami Iida [d], Seiichiro Ogawa [e], Yoshiyuki Suzuki [f], Kousaku Ohno [b], Eiji Nanba [a]

[a] Division of Functional Genomics, Research Center for Bioscience and Technology, Tottori University, 86 Nishi-cho, Yonago, 683-8503, Japan
[b] Division of Child Neurology, Tottori University Faculty of Medicine, 36-1 Nishi-cho, Yonago, 683-8504, Japan
[c] Department of Biomedical Regulation, School of Health Science, Faculty of Medicine, 86 Nishi-cho, Yonago, 683-8503, Japan
[d] Central Research Laboratories, Seikagaku Corporation, 3-1253, Tateno, Higashi-Yamato, Tokyo, 270-0021, Japan
[e] Department of Biosciences and Informatics, Faculty of Science and Technology, Keio University, Hiyoshi, Kohoku-ku, Yokohama, 223-8522, Japan
[f] International University of Health and Welfare Graduate School, 2600-1 Kita Kanemaru, Otawara, 324-8501, Japan

ARTICLE INFO

Article history:
Received 12 August 2010
Accepted 12 August 2010
Available online 18 August 2010

Keywords:
Chemical chaperone therapy
Lysosomal storage disease
Neurodegeneration
G_{M1}-gangliosidosis
β-galactosidase
Luciferase

ABSTRACT

β-Galactosidosis is a group of disorder based on heterogeneous mutations of GLB1 gene coding for the lysosomal acid β-galactosidase (β-gal). A decrease of the β-gal enzyme activity results in progressive accumulation of substrates in somatic cells, particularly in neurons, leading to severe neuronal dysfunction. We have previously reported that *N*-octyl-4-epi-β-valienamine (NOEV), a chemical chaperone compound, stabilized various mutant human β-gal proteins and increased residual enzyme activities in cultured fibroblasts from human patients. These data proved a potential therapeutic benefit of chemical chaperone therapy for patients with missense β-gal. This effect is mutation specific. In this study, we have established a sensitive luciferase-based assay for measuring chaperone effect on mutant human β-gal. A dinoflagellate luciferase (Dluc) cDNA was introduced to the C-terminus of human β-gal. When COS7 cells expressing the Dluc-tagged human R201C β-gal was treated with NOEV, there happened a remarkable increase of the mutant β-gal activity. In the presence of NH_4Cl, luciferase level in the medium increased in parallel with the enzyme activity in cell lysates. We also found that proteasome inhibitors enhance chaperone effect of NOEV. These results demonstrate that the luciferase-based assay is a reliable and convenient method for screening and evaluation of chaperone effects on human β-gal mutants, and that it will be a useful tool for finding novel chaperone compounds in the future study.

1. Introduction

Lysosomal acid β-galactosidase (β-gal, EC 3.2.1.23), encoded by GLB1 (3p21.33) in humans, hydrolyzes the terminal β-galactosyl residues from ganglioside G_{M1} and related glycoconjugates such as oligosaccharides derived from glycoproteins and keratan sulfate in somatic cells [1]. Allelic mutations of the gene result in excessive storage of the substrates in various cells and tissues. Genetic β-galactosidase deficiency (or β-galactosidosis) is a group of disorders including two clinically distinct diseases: G_{M1}-gangliosidosis (OMIM 230500) and Morquio B (OMIM 253010). Until now, more than 130 GLB1 gene mutations are collected [1–3]. G_{M1}-gangliosidosis is a generalized neurosomatic disease in children (infantile form, juvenile form), and rarely in adults (adult form). The abnormal storages of ganglioside G_{M1}, mucopolysaccharide keratan sulfate and glycoprotein-derived oligosaccharides are widely distributed in the central nervous system (CNS), skeletal system, and visceral organs. Morquio B disease (OMIM 253010) is a generalized skeletal dysplasia without neurological involvement.

At present only symptomatic and supportive therapy is available for the brain damage in human G_{M1}-gangliosidosis patients. Different strategies have been explored to treat this disease including allogenic bone marrow transplantation [4], gene therapy [5] and substrate reduction therapy [6]. These approaches are promising but still far from clinical application. The enzyme replacement therapy conducted for Gaucher disease and other lysosomal storage diseases is not available at present for β-galactosidosis [7].

Based on the study on mutant α-galactosidase A in Fabry disease [8], we proposed chemical chaperone therapy for brain pathology in G_{M1}-gangliosidosis, using an *in vitro* enzyme inhibitor *N*-octyl-4-epi-β-valienamine (NOEV), a chemical compound newly produced by organic synthesis, as a potent stabilizer of mutant β-gal in somatic cells

Abbreviations: β-gal, β-galactosidase; NOEV, *N*-octyl-4-epi-β-valienamine; Dluc, dinoflagellate luciferase; DMEM, Dulbecco's modified Eagle's medium; 4-MU, 4-methylumbelliferone.

* Corresponding author. Division of Functional Genomics, Research Center for Bioscience and Technology, Tottori University, 86 Nishi-cho, Yonago, 683-8503, Japan. Fax: +81 859 38 6470.
E-mail address: kh4060@med.tottori-u.ac.jp (K. Higaki).

1096-7192/$ – see front matter © 2010 Elsevier Inc. All rights reserved.
doi:10.1016/j.ymgme.2010.08.012

from patients with this disorder [9]. The experiments on patients' fibroblasts and model mice revealed remarkable restoration of mutant enzyme activity and reduction of the substrates storage. Oral treatment with NOEV in mice expressing human R201C mutation showed a decrease in CNS G_{M1} content and prevention of neurological deterioration [9,10]. The screening of NOEV effect on patients' fibroblasts conducted in our initial study indicated that the chemical chaperone effect is mutation specific [11].

Bioluminescence reporter proteins have been widely used to monitor biological events and gene expression [12]. Firefly luciferase is the most common reporter protein. However, it is not suitable for pharmacological assay in live cells because of the difficulties in controlling the intracellular concentrations of the substrates, luciferin, ATP and pH [13]. Several secretory luciferase proteins have recently been identified and emerged as powerful tools for continuous monitoring of biological events in live cells [14,15]. These proteins enable us to simply measure luciferase activities in the extracellular space as for monitoring the amount of the functional proteins [16].

In this study, we established a secreted dinoflagellate luciferase-based assay for measuring chaperone effect on mutant human β-gal to achieve a high throughput system for screening new chaperones.

2. Materials and methods

2.1. Materials

Dulbecco's Modified Eagle's Medium (DMEM) and DMEM without L-glutamine and phenol red were obtained from Wako (Tokyo, Japan). Fetal bovine serum (FBS) was from Hyclone (Waltham, MS, USA). Lipofectamine 2000 and Zero Blunt TOPO PCR Cloning Kit were purchased from Invitrogen (Carlsbad, CA, USA). 4-Methylumbelliferone-conjugated β-D-galactoside (4-MU-β-galactoside) was from Sigma (St. Louis, MO, USA). A dinoflagellate luciferase (Dluc) cDNA and its substrate were kindly provided from TOYO B-Net Co. Ltd (Tsukuba, Japan) [15]. Proteostasis regulators, MG132 and celasterol, were purchased from Calbiochem (La Jolla, CA, USA).

2.2. Chaperone compound NOEV

A chaperone compound for β-galactosidase, *N*-octyl-4-epi-β-valienamine (NOEV), was synthesized by modification of a glucocere brosidase inhibitor [9,17]. It is stable at room temperature and strongly inhibits human β-galactosidase *in vitro*. It is freely soluble in methanol or dimethyl sulfoxide, and soluble in water up to 3–5 mM at room temperature. The molecular weight is 287.40. Stock solution of NOEV was prepared in sterile dH_2O and stored at −30 °C.

2.3. Construction of β-gal-flag-Dluc expression plasmids

Human GLB1 (hGLB1) cDNA was subcloned into a mammalian expression vector, pCMV-script (Stratagene, La Jolla, CA, USA). A flag-epitope was introduced into the C-terminus of hGLB1 by PCR (β-gal-flag). Directional cloning was then carried out via restriction enzyme site: *Sac*I and *Xho*I, to introduce a Dluc cDNA [15] into the plasmid after the C-terminal flag (β-gal-flag-Dluc) (Fig. 1A). The following mutations were introduced by using the Quick Change site-directed mutagenesis Kit (Stratagene): I51T, R201C and R457Q. All the constructs were confirmed by direct sequencing.

2.4. Transient transfection

COS7 cells were cultured at 37 °C in 5% CO_2 in DMEM containing 10% FBS. For transient transfection, 2.5×10^5 cells were plated in 35-mm culture dish and incubated overnight. When the cells were 90% confluent, transient transfection was carried out with 4 μg of plasmid DNA (mock, wild type β-gal, I51T, R201C and R457Q) using Lipofectamine 2000 according to the manufacturer's protocol. Eight hours after transfection, the growth medium was changed into DMEM without phenol red containing 10% FBS with 0, 0.2 or 2 μM NOEV. Then the cells were further grown for 48 or 96 h before harvest. For the treatment of proteostasis regulators, cells were treated with 0, 0.2 or 2 μM NOEV in absence or presence of 0.1 μM MG132 or 2 μM cerasterol for 96 h.

2.5. β-Gal enzyme assay

Cells in 35 mm dishes were scraped into 200 μl of 0.1% Triton X-100 in dH_2O and were homogenized with pipetting. The samples were then centrifuged to remove insoluble materials. β-Gal assay was performed on 96-well plates. The enzyme assay mixture consisted of 10 μl supernatant of cell lysates and 20 μl substrate solution containing 1 mM of 4-MU-β-galactoside in 0.1 M citrate buffer (pH 4.5) and 0.1 M NaCl. After incubation for 30 min at 37 °C, the enzyme reaction was terminated by adding 0.2 M glycine-NaOH buffer (pH 10.7), and the liberated 4-MU was measured by fluorometry (excitation 355 nm; emission 460 nm, Infinite 200, Tecan Japan, Kawasaki, Japan) as described previously [11]. Protein concentration was determined with the Protein Assay Rapid Kit (Wako).

2.6. Western blot analysis and immunoprecipitation

Cells were scraped into ice-cold lysis buffer [50 mM Tris–HCl (pH 8.0), 150 mM NaCl and a protease inhibitor cocktail (Roche Diagnostics, Mannheim, Germany)] and lysed by sonication. Insoluble materials were removed by centrifugation at 3,700 rpm for 15 min at 4 °C and protein concentrations were determined with a Protein Assay Rapid Kit (Wako). Cell lysates (10 μg protein) were electrophoresed on a 10% SDS-PAGE and transferred to a PVDF membrane. The blots were probed with mouse monoclonal anti-flag M2 Ab (Sigma, 1:10,000) or rabbit polyclonal anti-β-gal Ab (#653, 1:2,000) [18] and developed with Amersham ECL Plus Western Blotting Detection Reagents (GE Healthcare Bio-Sciences KK, Tokyo, Japan). The immunoprecipitation was carried out with anti-flag M2 Ab using Catch and Release v2.0 kit (Upstate, Charlottesville, VA, USA) according to the manual.

2.7. In vitro stabilization of β-gal

In vitro stabilization of recombinant β-gal-flag-Dluc protein by NOEV was examined as previously [19]. Briefly, anti-flag immunoprecipitates from COS7 cells expressing β-gal-flag-Dluc (20 μl, pH 7.4) were incubated with NOEV (0, 0.02, 0.2 or 2 μM) on ice. The samples were heated at 48 °C for 20, 40 or 60 min, then the enzyme assay was performed as described above at pH 5.0.

2.8. Bioluminescence assay

COS7 cells was cultured in 35 mm dishes with DMEM containing 10% FBS for 24 h, and then transfected with luciferase reporter constructs: The medium was changed into 1 ml DMEM/10% FBS without phenol red containing NH_4Cl (0 or 20 mM) and NOEV (0, 0.2 or 2 μM). After 48 h, the cells were harvested with cell lysis buffer (TOYO B-net) and the medium were collected as well. The luciferase activities in cell lysates and medium were determined using specific substrate from Toyo Ink [15] and measured by chemiluminescencer AB2000 (ATTO, Tokyo, Japan) and expressed in arbitrary units (A.U.). pEGFP-N1 plasmid (Clontech, Mountain View, CA, USA) was used as an internal transfection control for each experiment.

2.9. Statistical analysis

Student *t* test were performed using a StatView software with $p<0.05$ regarded as statistically significant.

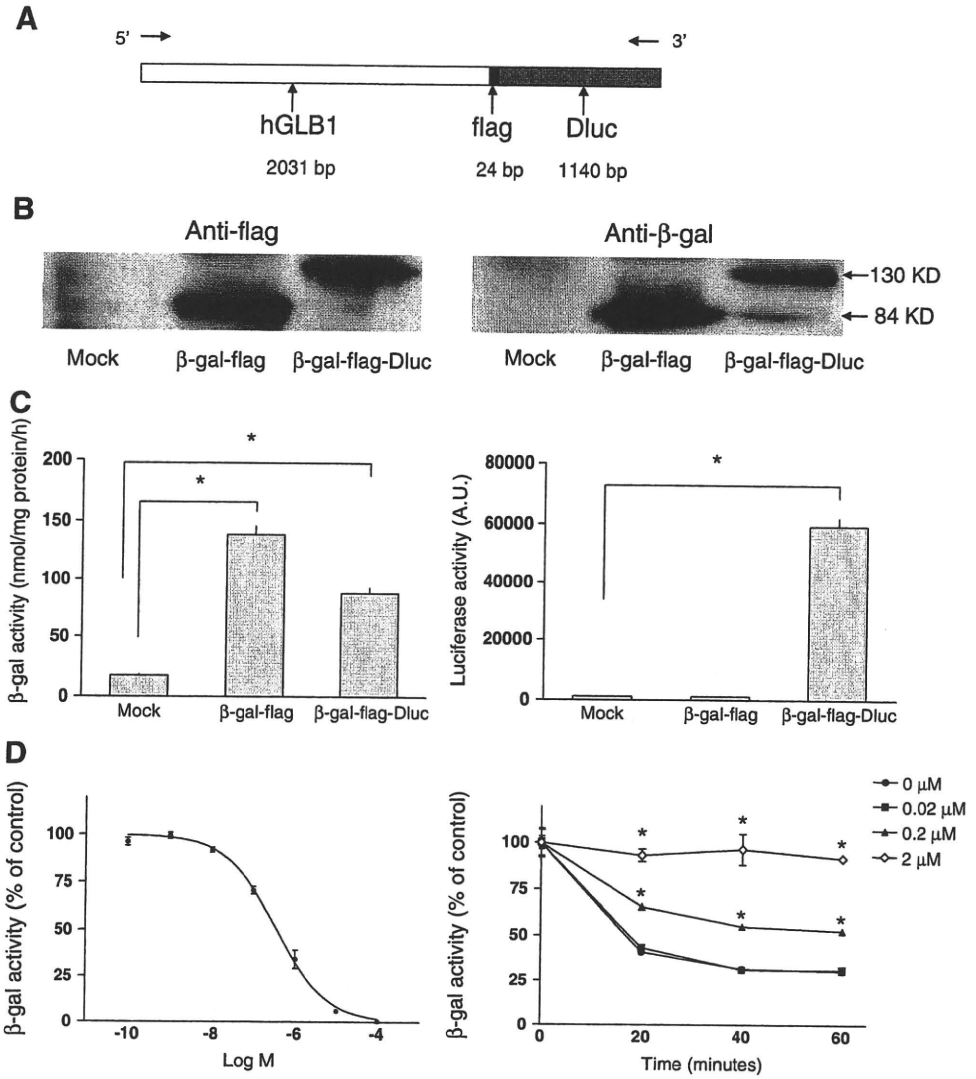

Fig. 1. Characterization of the recombinant β-gal-flag-Dluc. (A) Plasmid constructs. Flag epitope and dinoflagellate luciferase (Dluc) were introduced into the C-terminal hGLB1 cDNA right before the stop codon (β-gal-flag-Dluc). Another plasmid carrying hGLB1 only with flag epitope was also constructed (β-gal-flag). (B) The expression of β-gal-flag and β-gal-flag-Dluc was detected in cell lysate from transiently transfected COS7 cells by western blotting. 130 KD product was the recombinant β-gal-flag-Dluc, and the 84KD was endogenous β-gal precursor. (C) β-Gal and luciferase activity in cell lysates from transiently transfected COS7 cells. (D) The inhibition (left) and heat stability (right) effect of NOEV on immunoprecipitate β-gal-flag-Dluc protein from transiently transfected COS7 cell lysate. Each point represents the mean ± SEM of three determinations each done in triplicate.

3. Results

3.1. Characterization of recombinant β-gal-flag-Dluc protein

To test functional relevance of Dluc-tagged normal human β-gal proteins, flag-tagged human β-gal cDNA (β-gal-flag) and flag-Dluc-tagged β-gal (β-gal-flag-Dluc) were transiently expressed in COS7 cells and cell lysates were collected 24 h later. Both β-gal-flag and β-gal-flag-Dluc proteins were detected in the lysates by anti-flag and anti-β-gal western blots (Fig. 1B). The β-gal enzyme activity was detected in the lysates both from β-gal-flag and β-gal-flag-Dluc transfected cells, whereas the luciferase activity was detected only in β-gal-flag-Dluc lysates (Fig. 1C). When lysates from β-gal-flag-Dluc transfected cells were incubated with NOEV at pH 5, NOEV caused dose-dependent inhibition of the β-gal activity (Fig. 1D left) [11]. β-Gal-flag-Dluc protein was stabilized by NOEV dose-dependently under heat inactivation condition (Fig. 1D right), suggesting that NOEV binds to these recombinant proteins *in vitro*.

3.2. Secretion of lysosomal β-gal in the presence of NH_4Cl

Lysosomal enzymes have been shown to be synthesized as microsomal precursors, and then processed to mature enzymes in the lysosomes. NH_4Cl, a lysosomotropic drug, causes extensive secretion of both precursor and mature forms of lysosomal β-gal protein [20]. To see whether active β-gal was detectable in the medium after a treatment with NH_4Cl, COS7 cells expressing the recombinant enzymes were treated with or without 20 mM NH_4Cl, and β-gal enzyme assay was performed using both the lysates and the medium. NH_4Cl treatment caused a clear reduction in the enzyme activity in the lysates, which was accompanied with an increase in the medium (Fig. 2A). Similarly, treatment of the cells expressing β-gal-flag-Dluc showed a decrease of luciferase activities in the cell lysate and an increase in the medium (Fig. 2B). We then examined whether the chaperone effect of NOEV on β-gal-flag-Dluc protein was detectable by measuring luciferase activity in the medium. 0.2 and 2 μM NOEV increased both β-gal activity in the lysate and luciferase

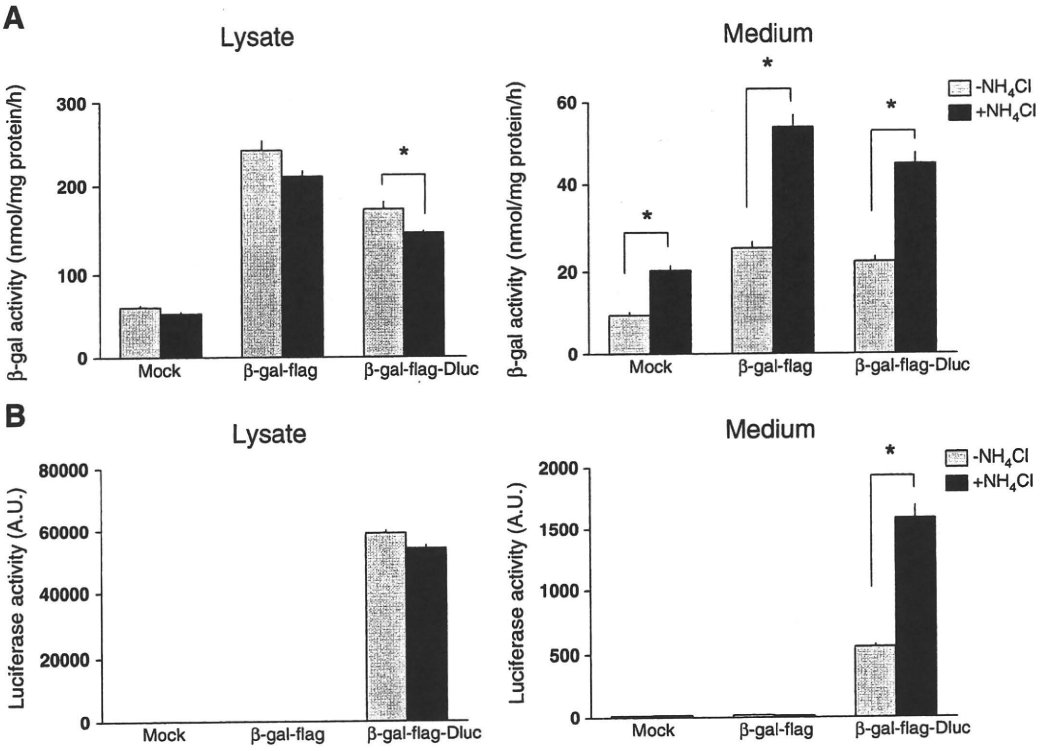

Fig. 2. NH_4Cl secretes β-gal-flag-Dluc protein into the medium. The transiently transfected COS7 cells were cultured for 48 h in the absence or presence of 20 mM NH_4Cl. The β-gal (A) and luciferase (B) activities were estimated in cell lysates and medium as described in materials and methods. Each bar represents the mean ± SEM of three determinations each done in triplicate. *$p<0.05$, statistically different from the values in the absence of NH_4Cl.

activity in the medium from β-gal-flag-Dluc transfected COS cells treated with NH_4Cl (Fig. 3). We observed no adverse effect of NH_4Cl on proliferation of COS7 cells (data not shown).

3.3. NOEV effects on mutant β-gal proteins

Mutant β-gal-flag-Dluc constructs harboring R457Q and two of the most common mutations in Japanese patients: I51T (for adult G_{M1}) and R201C (for juvenile G_{M1}), were engineered by Quick Change site-directed mutagenesis. Our previous study on patients' fibroblasts showed the capacity of NOEV to restore enzyme activities of R201C and R457Q but not that of I51T. [11]. In the COS7 cells transiently expressed with mutant β-gal-flag-Dluc constructs, NOEV caused significant increase of β-gal activity in the cell lysates (Fig. 4A). The maximum response was obtained at 2 μM of R201C and 0.2 μM of R457Q. NOEV was ineffective for I51T β-gal-flag-Dluc as expected from our previous findings on patients' fibroblasts [11]. Given NH_4Cl-induced secretion of lysosomal β-gal, we examined whether NOEV effect was reflected in the luciferase activity in the medium, after an exposure of the cells to NH_4Cl. The luciferase activity was barely detectable in the medium from mock transfected cells. There emerged considerable levels of luciferase activity in the medium, when cells were transiently expressed with the mutants β-gal-flag-Dluc constructs. NOEV caused significant increases in the luciferase activities in the medium of cells expressing with R201C and R457Q but not with I51T (Fig. 4B).

Most mutant proteins with missense mutations were degraded in the endoplasmic reticulum (ER) [11]. Therefore, proteostasis regulators are thought to enhance the chaperone effect [21]. We have examined two proteostasis inhibitors (cerasterol and MG132) to investigated the effects on mutant R201C enzyme and revealed that both increased the enzyme activity to 112% and 114% without NOEV; 152% and 141% with 0.2 μM NOEV; 154% and 164% with 2 μM NOEV, comparing with cells treated only with growth medium, respectively (Table 1). Strikingly, co-administration with MG132 and 0.2 μM NOEV reached almost same level that 2 μM NOEV achieved. Additionally, 2 μM NOEV restored about 20% higher enzyme activity with additional celasterol. These effects were well reproduced by luciferase assay using mediums, again proving that luciferase activities can represent the enzyme activities.

4. Discussion

In this study, we developed a sensitive luciferase-based assay for evaluate a chemical chaperone effect on human mutant β-gal. The luciferase activity in the medium faithfully mirrored in the β-gal activity in cell lysates, indicating that our luciferase-tagged construct can be a good tool for chaperone effect screening.

β-Gal gene mutations result in abnormal accumulation of various substrates and different clinical phenotypes: G_{M1}-gangliosidosis and Morquio B. Some mutant proteins are unstable at neutral pH in the endoplasmic reticulum and the Golgi apparatus and are rapidly degraded without appropriate or correct molecular folding [22,23]. Exogenously supplied chemical compounds that inhibit enzyme activity *in vitro* bind to the enzyme intracellularly to form a complex, and then stabilize the protein during transport to the lysosome. The complex then dissociates under the acidic condition in the lysosome, and the mutant enzyme remains stabilized and functional. These inhibitor candidates can restore mutant lysosomal enzyme activity.

As a proof of this concept, NOEV has been shown to markedly increase the mutant enzyme activities about one-third of the cultured fibroblast strains from G_{M1}-gangliosidosis patients [11]. It was active in cells mainly from juvenile form and some infantile form patients. Several compounds have recently been identified as potential chaperones for other lysosomal storage diseases [24,25]. Based on the concept of chemical chaperone effects, most of the successful chaperones were first identified as competitive inhibitors of their